Palaeogeography, Palaeoclimatology, Palaeoecology 577 (2021) 110539

Contents lists available at ScienceDirect

Palaeogeography, Palaeoclimatology, Palaeoecology

journal homepage: www.elsevier.com/locate/palaeo

Paleoclimate and paleoenvironment reconstruction of paleosols spanning the Lower to Upper Cretaceous from the Rukwa Rift Basin, Tanzania

Theresa J. Orr [a,*], Eric M. Roberts [b], Christopher M. Wurster [a], Cassy Mtelela [c], Nancy J. Stevens [d,e], Patrick M. O'Connor [d,e]

[a] Earth and Environmental Sciences, James Cook University, Cairns, QLD 4870, Australia
[b] Earth and Environmental Sciences, James Cook University, Townsville, QLD 4811, Australia
[c] Department of Geosciences, University of Dar es Salaam, Dar es Salaam, Tanzania
[d] Department of Biomedical Sciences, Ohio University, Athens, OH 45701, USA
[e] Center for Ecological and Evolutionary Studies, Ohio University, Athens, OH 45701, USA

ARTICLE INFO

Editor: Isabel Montanez

Keywords:
Africa
Pedogenic carbonate
Stable isotope
Paleosol geochemistry
Pedogenesis
Cretaceous paleoclimate

ABSTRACT

The Cretaceous Period is considered the archetypical greenhouse interval, yet there is mounting evidence for intermittent cooler climatic phases throughout this geologic span. Few continental climate histories exist for the Cretaceous south of the paleoequator, and fewer still for Africa during this time. The Cretaceous Galula Formation is one of the few exposed fossiliferous continental sedimentary successions from what is now subequatorial Africa that also contains paleosols and spans both the Early and Late Cretaceous series. Bulk sediment and pedogenic carbonate nodules were sampled from paleosols located throughout ~500 m of the Galula Formation stratotype section, including four from the lower Mtuka Member (Aptian-Cenomanian) and four from the upper Namba Member (Cenomanian-Campanian), to reconstruct the paleoclimate and paleoenvironment of the Rukwa Rift Basin. The Mtuka paleosols developed on channel fill deposits in a semi-arid climate amidst well-defined wet and dry seasons that predominantly generated vertic Calcisols. Geochemical and morphological climofunctions determined that mean annual precipitation (MAP) increased up-section from 454 to 860 mm/yr, whereas the $\delta^{18}O$ values of pedogenic carbonates and Bt horizon major-element paleothermometry estimated mean annual temperature (MAT) remained relatively steady, ranging between 12.9 and 13.9 °C throughout the Mtuka Member. The paleosols of the overlying Namba Member formed on channel fill and overbank deposits proximal to the main channels, in a semi-arid to sub-humid climate with little seasonality, forming mostly calcic Argillisols. The Namba paleosols formed under slightly wetter and cooler conditions, recording MAP values between 602 and 987 mm/yr, and MAT estimates between 10.3 and 12.5 °C. These data are consistent with the Mtuka paleosols corresponding to the cool greenhouse period that spanned the Aptian-Albian, with the Namba paleosols corresponding to Late Cretaceous cooling following the Cretaceous Thermal Maximum. This work demonstrates that temperate conditions prevailed in the Rukwa Rift Basin during the mid-Late Cretaceous.

1. Introduction

The Cretaceous has long been considered a greenhouse interval, although whether this climate mode was enduring or episodic is less clear. Cretaceous climate reconstructions are predominantly derived from marine records (Gao et al., 2015), because terrestrial climate records are generally limited or incomplete (Huang et al., 2012; Gao et al., 2015; but see Pearson et al., 2004; Bowman et al., 2013). Paleosols (fossil soils) reflect climate in terrestrial settings, recording atmospheric, climatic, and environmental conditions during the life of the soil (Tabor and Myers, 2015; Driese and Ashley, 2016; Varela et al., 2018). Paleosol composition and morphology form the basis of many proxies used to qualitatively and quantitatively reconstruct paleoclimate and paleoenvironment (Sheldon and Tabor, 2009; Tabor and Myers, 2015).

Recent paleosol research, using stable isotope values of pedogenic carbonates, suggests low atmospheric CO_2 concentrations and temperatures during the Early Cretaceous (e.g. Huang et al., 2012; Li et al., 2016). Yet conflicting climate reconstructions have been recovered for

* Corresponding author at: College of Science and Engineering, James Cook University, 14-88 McGregor Road, Smithfield, QLD 4878, Australia.
E-mail addresses: theresa.orr@my.jcu.edu.au (T.J. Orr), eric.roberts@jcu.edu.au (E.M. Roberts), christopher.wurster@jcu.edu.au (C.M. Wurster), stevensn@ohio.edu (N.J. Stevens), oconnorp@ohio.edu (P.M. O'Connor).

https://doi.org/10.1016/j.palaeo.2021.110539
Received 27 January 2021; Received in revised form 13 June 2021; Accepted 20 June 2021
Available online 25 June 2021

the Late Cretaceous, with studies documenting both low pCO_2 values and temperatures (e.g. Li et al., 2020), and warm greenhouse conditions (e.g. Nordt et al., 2003; Salazar-Jaramillo et al., 2019), with the possibility of an episodic climate mode, rather than a monotonic increase or decrease in pCO_2 and temperature throughout the geologic period (e.g. Nordt et al., 2003; Huang et al., 2012). Indeed, other lines of evidence (e.g. foraminiferal oxygen isotope records), suggest lower pCO_2 and temperatures in the Early Cretaceous, followed by a mid-Cretaceous peak with a Cretaceous Thermal Maximum (KTM) proposed in the Turonian (Huber et al., 2018). Few studies have quantified paleosols spanning the Early-Late Cretaceous transition; hence additional reliable continental climate archives are required to improve our understanding of climate dynamics in the mid-Cretaceous.

The Cretaceous climate record of continental Africa is less well-documented than other landmasses, particularly from deposits south of the equator. This issue is in part due to an extreme paucity of accessible/exposed Cretaceous strata. In recent decades, renewed interest in older depositional systems within the East African Rift System (EARS) has resulted in the discovery of reasonably extensive Cretaceous rift-deposits underlying younger EARS successions (e.g. Jacobs, 1990; Roberts et al., 2004, 2010; Agyemang et al., 2019). Many of these pre-EARS rift-fill successions are linked with the separation of Africa from South America (Roberts et al., 2010) and the opening of the south Atlantic Ocean (Guiraud et al., 1992) during the continued break-up of Gondwana. In particular, the Rukwa Rift Basin in southwestern Tanzania (Fig. 1) has been the subject of intensive sedimentological and paleontological exploration, resulting in the identification and characterization of a trans-continental braidplain-fluvial-floodplain system formalized as the Galula Formation. The Galula Formation hosts a diverse faunal assemblage, including nonavian dinosaurs (O'Connor et al., 2006; Gorscak et al., 2014, 2017), notosuchian crocodyliforms (O'Connor et al., 2010; Sertich and O'Connor, 2014) and a gondwanatherian mammal (O'Connor et al., 2019), highlighting the paleobiological importance of these strata. Lithified paleosols identified in the Galula Formation provide an opportunity to better constrain the depositional paleoenvironment that sustained both freshwater and terrestrial vertebrate faunas in this segment of the Rukwa Rift Basin.

This study explores the geochemistry and macromorphological characteristics of paleosols from across the Cretaceous Galula Formation in order to constrain paleoclimate and paleoenvironment at the time of deposition. Previous interpretations of Galula Formation paleoclimate and paleoenvironment are based solely on sedimentology and paleontology (e.g. O'Connor et al., 2006; Roberts et al., 2010). Paleopedological approaches are used to refine interpretations, with assessment of multiple paleosol horizons generating a high-resolution paleoclimate record for this region of continental Africa during the Cretaceous.

2. Background and geological setting

The Rukwa Rift is a ~ 300 km long by ~50 km wide NW-SE trending half-graben basin (Kilembe and Rosendahl, 1992; Kjennerud et al., 2001), located in the Western Branch of the EARS (Chorowicz, 2005).

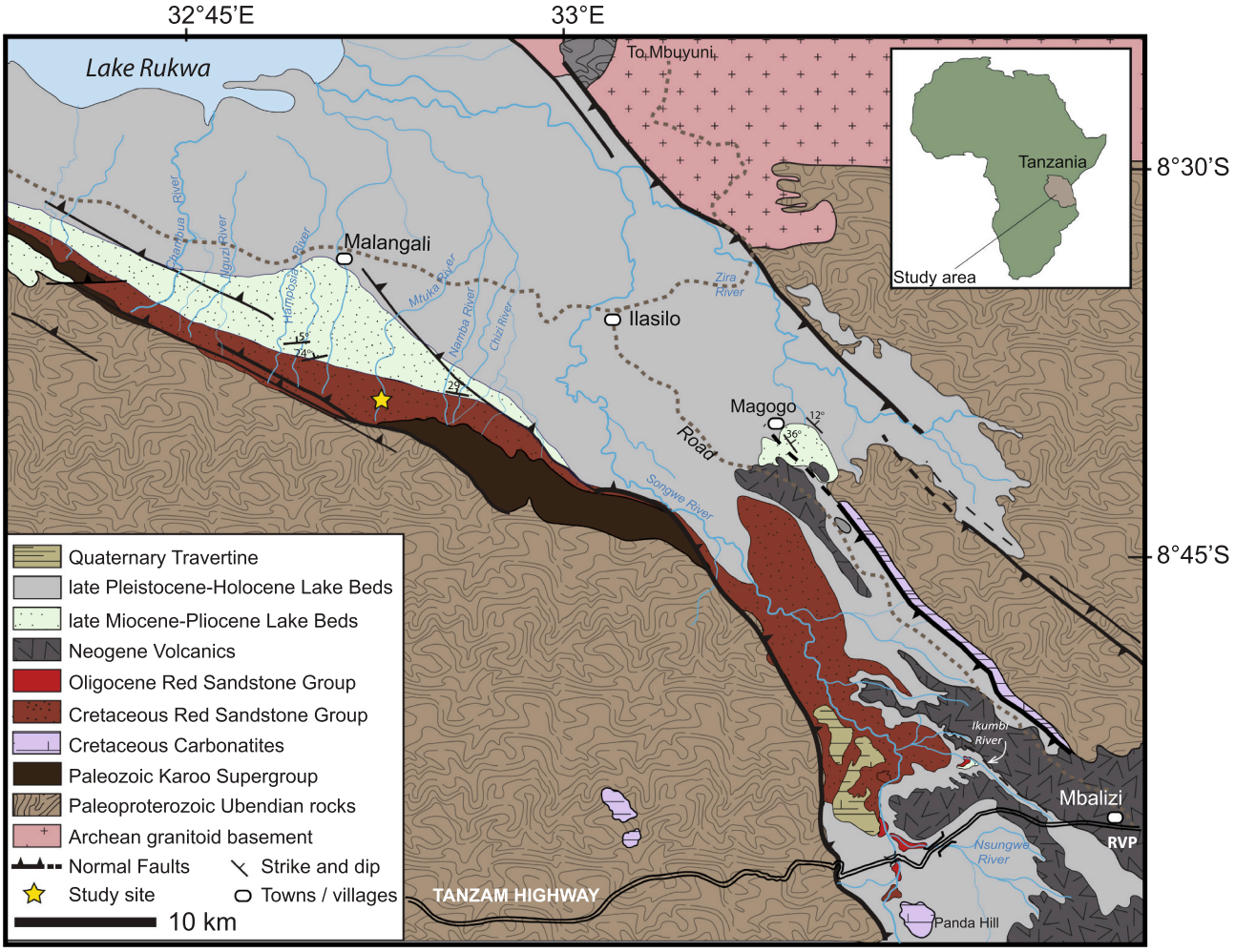

Fig. 1. Geologic map of the southern Rukwa Rift Basin, modified after Mtelela et al. (2017). Yellow star indicates sampling location. (For interpretation of the references to colour in this figure legend, the reader is referred to the web version of this article.)

The center of the basin is occupied by the 165-km-long Lake Rukwa (Kjennerud et al., 2001). Rift-fill sediment successions in the basin are the thickest in the EARS and some of the thickest in Africa, ranging in extent from 8 to 11 km (Kilembe and Rosendahl, 1992). These successions correspond to four distinct tectono-sedimentary phases, from older to younger forming the Upper Paleozoic Karoo Supergroup, the Cretaceous Galula Formation, the Oligocene Nsungwe Formation and the Miocene-Recent Lake Beds strata (Roberts et al., 2012) (Fig. 1). To date, the majority of geological investigations on the Rukwa Rift have focused on the structural and tectonic evolution of the basin (e.g. Ebinger, 1989; Ebinger et al., 1989; Kilembe and Rosendahl, 1992; Morley et al., 1992; Rosendahl et al., 1992; Delvaux et al., 1998). However, well-exposed, richly fossiliferous rift-fill deposits have more recently been the subjects of extensive stratigraphic and paleontologic investigations (e.g. Roberts et al., 2004, 2012, 2016; Stevens et al., 2005, 2006, 2008, 2009, 2013; O'Connor et al., 2006, 2010, 2019; Hilbert-Wolf and Roberts, 2015; Hilbert-Wolf et al., 2016, 2017; Mtelela et al., 2016, 2017; Lawrence et al., 2020).

The Galula Formation variably overlies Paleoproterozoic metamorphic rocks or the Upper Paleozoic Karoo Supergroup, and was deposited by a braided fluvial system during continent-wide tectonic activity associated with the break-up of Gondwana (Roberts et al., 2010). Through sedimentological and stratigraphic analysis, Roberts et al. (2010) divided the Galula Formation into a lower (Mtuka) and upper (Namba) member. The Mtuka Member encompasses the basal ~170 m of the Galula Formation and intermittently crops out along river drainages in the Tukuyu, Galula, and Usevia areas, located from south to north along the axis of the rift (Roberts et al., 2010). The Mtuka Member is characterized by abundant conglomerates and paleosols, coarse-grained sandstones, thick overbank deposits of mudstone, and major fluvial erosion surfaces (Roberts et al., 2010). The Namba Member represents the upper ~350 m of the Galula Formation and is exposed along the same river drainages as the Mtuka Member, with the addition of the main Songwe field area (Fig. 1), located in the southern end of the basin (Roberts et al., 2010). The Namba Member is finer grained than the Mtuka Member and is defined by homogenous fine- to medium-grained sandstones, with subordinate mudstones (Roberts et al., 2010).

The Mtuka and Namba members host a rich fossil assemblage, with a diversity of crocodyliforms and sauropod dinosaurs (O'Connor et al., 2010; Gorscak et al., 2014, 2017; Sertich and O'Connor, 2014), along with rare theropod dinosaurs, fish and turtles (O'Connor et al., 2006). The majority of the fossils collected to date derive from the Namba Member, although limited vertebrate remains are known from the Mtuka Member. The Namba Member has also produced the most complete Cretaceous mammal from all of continental Africa, represented by the gondwanatherian mammal *Galulatherium jenkinsi* (O'Connor et al., 2019). The discovery of vertebrate fossils from a period of basin development coincident with the separation of Africa from South America and the opening of the Atlantic Ocean (Guiraud et al., 1992), emphasizes their paleontological importance. However, accurate temporal refinement of the Galula Formation has been impeded by a lack of suitable material for radiometric dating. Previous age assignments relied on biostratigraphy (e.g. Gottfried et al., 2004; O'Connor et al., 2006), and sediment deposition considered correlative with the Aptian Dinosaur Beds of Malawi and partially coeval with mid-Cretaceous carbonatite intrusions (Fawley and James, 1955; Roberts et al., 2010). A recent magnetostratigraphic study of the Galula Formation (Widlansky et al., 2018) provided important new age constraints, and consigned the Mtuka Member to the Aptian-Cenomanian and the Namba Member to the Cenomanian-Campanian.

Southern hemisphere continental paleoclimate records of the mid-Cretaceous are scarce, and currently rely heavily on fossil evidence (e.g. paleofloral assemblages; Varela et al., 2018). The improved age constraint of the Galula Formation enables better understanding of the climatic and environmental information contained within the paleosols of the Mtuka and Namba members. Sedimentological evidences suggest a climatic shift from semi-arid to sub-humid conditions in the Mtuka and Namba members, respectively. Evidence for the climatic shift includes clay mineralogy shifts, decreasing pedogenic carbonate abundances, and mild sandstone petrological changes between the Mtuka and Namba members (Roberts et al., 2010). High-resolution paleoclimate records from multiple paleosol horizons in the Mtuka and Namba members are reported here to help fill this knowledge gap.

3. Methods

3.1. Field investigations

The study area is located ~50 km northwest of the town of Mbeya in southwestern Tanzania (8.8978°S 33.4467°E). Paleosols were identified in measured sections of the Galula Formation in natural exposures along the Mtuka River (Fig. 1). Profiles were described in detail and classified, with taxonomic nomenclature incorporating the order and profile classifications of Mack et al. (1993) and Marriott and Wright (1993). Paleosol horizons and mottle colors were described using the Munsell Color (2009) chart. Pedogenic features were described for each horizon, including argillans, mineral accumulations, mottles, peds, rhizoliths, vadose textures, and vertic morphologies (e.g. Gile et al., 1966; Klappa, 1980a, 1980b; Mack et al., 1993; Birkeland, 1999). For paleosols with Bk horizons, the depth to carbonate horizon (DTC) was recorded and adjusted using depth of burial estimates from stratigraphic evidence and the compaction equation of Sheldon and Retallack (2001). The thickness of soil with carbonates was also recorded and similarly adjusted. Whole rock samples were collected from horizons in each paleosol profile.

3.2. Laboratory

The Bt horizon of each paleosol was sampled and subsequently prepared by a commercial laboratory (Vancouver Petrographics, Ltd.) as standard thin-sections. The thin-sections were examined via petrographic microscopy. Samples were analyzed for major and trace elements at the Advanced Analytical Centre (AAC) at James Cook University. Samples were crushed using a Rocklabs BenchTop Ring Mill. Loss on ignition (LOI) of the samples was carried out in a Labec CEMLL-SD muffle furnace at 1000 °C for 4 h. Glass discs were then prepared using 1 g of sample and 8 g of 12:22 Lithium Tetraborate/Lithium Metaborate flux, and fused in an Initiative Scientific F-M4 Fusion Bead Casting Machine. Major element composition was measured on a Bruker S2 PUMA X-ray fluorescence (XRF) spectrometer, using SpectraPlus. Trace elements were determined using a Teledyne Cetac Analyte G2 193 nm Excimer Laser Ablation unit connected with a Varian 820-ICP-MS. Laser energy was set at 3 J/cm^2, with a 85 μm laser beam size and 5 Hz repetition rate. Ca was measured by XRF and used as the internal standard for quantification purposes. Results were reported as oxide weight percentages (major) or ppm (trace), which were normalized to their molecular weights.

Samples from each paleosol were analyzed for clay mineralogy by the Central Analytical Research Facility at the Queensland University of Technology using X-ray diffraction (XRD). Clay minerals were identified using a PANalytical X'Pert Pro powder diffractometer and cobalt Kα radiation operating in Bragg-Brentano geometry. Data was processed using JADE (V2010, Materials Data Inc.), EVA (V5, Bruker) and X'Pert Highscore Plus (V4, PANalytical) with various reference databases (PDF4+, AMCSD, COD) for phase identification. Rietveld refinement was performed using TOPAS (V6, Bruker). XRD data are reported as weight percentages with a detection limit of 1 wt%.

Pedogenic carbonate nodules were collected from each paleosol when present. Micritic samples were extracted from each nodule and crushed using a Ring Mill. Zirconium crucibles were cleansed with hydrochloric acid and ashed sand (1000 °C > 4 h), and then washed with deionised water and ethanol prior to loading with samples. Stable oxygen isotope compositions were determined using a Thermo Scientific

GasBench III gas preparation and introduction system coupled to a DeltaV^{PLUS} isotope ratio mass spectrometer via the ConFloIV (AAC's Environmental Isotope Laboratory, James Cook University). Carbon dioxide was evolved from carbonate by reaction with 100% orthophosphoric acid in 15 mL Exetainer vials after atmosphere was replaced with He. Replicate samples of international standards NBS-18 ($\delta^{18}O = -23.2 \pm 0.1‰$) and NBS-19 ($\delta^{18}O = -2.20‰$ (defined)) with similar mass to unknown samples provided monitoring of accuracy and precision. Precisions (1σ) for reference materials (NBS-18 and NBS-19) were better than 0.1‰. $\delta^{18}O$ values are reported relative to Vienna PeeDee Belemnite (VPDB), by normalization with NBS-18 and NBS-19, unless stated otherwise.

3.3. Weathering ratios

Molecular weathering ratios were used to evaluate the extent of chemical weathering in each paleosol. The degrees of calcification (CAL = $(CaO + MgO)/Al_2O_3$), clayeyness (Clayeyness = Al_2O_3/SiO_2), hydrolysis (Hydrolysis = $Al_2O_3/(CaO + MgO + K_2O + Na_2O)$), leaching (L = Ba/Sr), oxidation (OX = Total Fe/Al_2O_3) and salinization (SAL = $(K_2O + Na_2O)/Al_2O_3$) were calculated to determine the dominant pedogenic processes, with the totality of weathering in each paleosol quantified by the chemical index of alteration (CIA = $100\times(Al_2O_3/Al_2O_3 + CaO + Na_2O + K_2O)$), paleosol weathering index (PWI = $100\times(4.20Na + 1.66\ Mg + 5.54\ K + 2.05Ca)$) and rare earth element (REE) trends. Weathering ratios were applied according to Nesbitt and Young (1982), Retallack (2001, 2003), Sheldon (2006a), Sheldon and Tabor (2009) and Gallagher and Sheldon (2013). Briefly, non-calcareous soils are indicated by CAL < 2, heavily leached soils by L > 2, and salinized soils by SAL > 2; ferruginous or oxic soils typically have OX > 1.2 (Retallack, 2001). McLennan (2001) classified CIA values <50 as unweathered rocks and values of 50–60, 60–80 and 80–100 as indications of incipient, moderate and intense weathering and pedogenesis, respectively. High PWI values represent poorly developed soils and low PWI values that of mature soils, with unweathered rocks plotting at or above 60 (Gallagher and Sheldon, 2013). REE were normalized (N) to Post-Archean Australian Shale (PAAS) (Taylor and McLennan, 1985), with a $La/Lu_{(N)} < 1$ indicative of neutral to mildly alkaline conditions and $La/Lu_{(N)} > 1$, acidic conditions (Bau, 1991). A negative ΣREE deviation from parent indicates acidic weathering and high fluid rock interaction, while a positive Eu/Eu* deviation represents reducing and low pH conditions during soil formation (Mohanty and Nanda, 2016). Provenance was calculated using the Ti/Al ratio of Maynard (1992), and REE concentrations following the method of Sheldon (2006b) and Mohanty and Nanda (2016).

3.4. Climofunctions

Paleoclimate reconstruction was achieved through a multi-proxy approach. The complex nature of biological, chemical and physical interactions within a soil demands the use of multiple proxies, with each founded on a different paleosol aspect (e.g. morphology, matrix elemental composition and carbonate stable isotope values) to capture an accurate overview of the paleoclimate. Mean annual precipitation (MAP) was estimated using the CALMAG (Nordt and Driese, 2010) and CIA minus potash (CIA-K) climofunctions, the PPM1.0 model (Stinchcomb et al., 2016) and the depth to carbonate (DTC) universal equation of Retallack (2005). Each geochemical climofunction has its own limitations; the CIA-K was exclusively applied to Bt horizons that contained <5 wt% bulk carbonate, and the CALMAG proxy only to those paleosols with vertic features. The DTC-MAP relationship was only applied to paleosols that exhibited full profiles (viz. retained A–horizons). Paleoprecipitation seasonality was determined using the mean annual range in precipitation (MARP) function of Retallack (2005), which is based on the thickness of soil with carbonate nodules (in cm). The aridity index of Köppen (1923) was also used. Mean annual temperature (MAT) was estimated using the PPM1.0 model, the salinization-based (Sheldon et al., 2002) and PWI-based (Gallagher and Sheldon, 2013) climofunctions, and the stable isotope – pedogenic carbonate relationship of Hyland and Sheldon (2013), modified after Dworkin et al. (2005).

4. Results

4.1. Mtuka Member

4.1.1. Macromorphology

Four paleosols (Mtuka 1–4) were identified and described from the Mtuka Member, with detailed descriptions of each profile reported in the Supplementary Materials online. The paleosols are hosted in red (2.5YR 3/6–4/8), fine-grained, moderately well-sorted, subarkosic sandstones and stratigraphically located between deep red to purple tabular sandstone units that often exhibit planar or trough cross-bedding, and erosional contacts (Fig. 2). Mtuka 1, 2 and 4 are single isolated profiles and are considered simple profiles, whereas Mtuka 3 is a composite profile that exhibits a complex succession of soils with extensive B-horizon overprinting (Fig. 3). The profiles of Mtuka 1 and 4 appear to have been preserved in full; whereas, Mtuka 2 and 3 are truncated by erosional surfaces. Soil structure is predominantly angular blocky, with rare instances of crumb and prismatic fabric in the upper horizons of Mtuka 1 and 2 (Table 1). Horizonation, with clear boundaries, is well developed in each unit (Table 1). Pedogenic carbonates range from filamentous accumulations (stage I) to layers of coalesced nodules (stage III) and indurated calcic horizons (stage IV), with stage II nodules (0.2–2 cm) observed in all profiles. The profiles contain evidence of bioturbation, including sediment infilled burrows and clay-lined rhizoliths with calcium carbonate accumulation and rare instances of spar (Fig. 4; Table 1). Root casts, root molds and rhizocretions are the most common forms of root traces observed. Greenish-grey mottling pervades most burrows and root traces, with cm-thick discrete bands extending across many of the profiles. Grey rhizohaloes containing cubic crystalline and diffuse hematite accumulations within root channels are isolated to Mtuka 1 (Fig. 4). Argillic features (e.g. grain, ped and vugh argillans) and vertic features (slickensides; Fig. 4E) are present in all profiles. The abundant stage II – IV carbonate accumulations and frequent vertic features (e.g. slickensides) categorize the Mtuka paleosols as predominantly vertic Calcisols, with the exception of Mtuka 2 (vertic Argillisol).

4.1.2. Micromorphology

Examination of thin sections confirmed pedogenic features that were observed at the macroscale in the field. Micromorphological features of all four Mtuka paleosols include predominantly angular blocky ped structure, calcium carbonate nodules and bioturbation (Fig. 4I-L). The coarse fraction is composed principally of quartz and feldspar, with trace heavy minerals, detrital Fe-Ti oxide grains and lithic fragments (Fig. 4L). Rhizoliths are abundant and frequently replaced by calcium carbonate (Fig. 4I); however microscopic accumulations of Fe-oxide along root channels are also observed (Fig. 4K). A clay-rich paleosol matrix is visible in the Mtuka 2 thin section, with rare instances of siderite (Fig. 4J).

4.1.3. Composition

The clay mineralogy of the vertic Calcisols (Mtuka 1, 3 and 4) is dominated by beidellite (28–75%), montmorillonite (15–30%), illite (9–20%) and palygorskite (< 1–16%), with minor proportions of kaolinite (3–6%). The sole vertic Argillisol (Mtuka 2) is dominated by montmorillonite (82%) and palygorskite (10%), with minor illite (7%) and kaolinite (1%).

Weathering ratio calculations for the Mtuka paleosols are provided in Fig. 5. Application of the CIA and PWI identified incipient to weak weathering in Mtuka 1, 3 and 4 and moderate weathering in Mtuka 2. CIA values range from 21 to 83, with a mean greater than 60 limited to

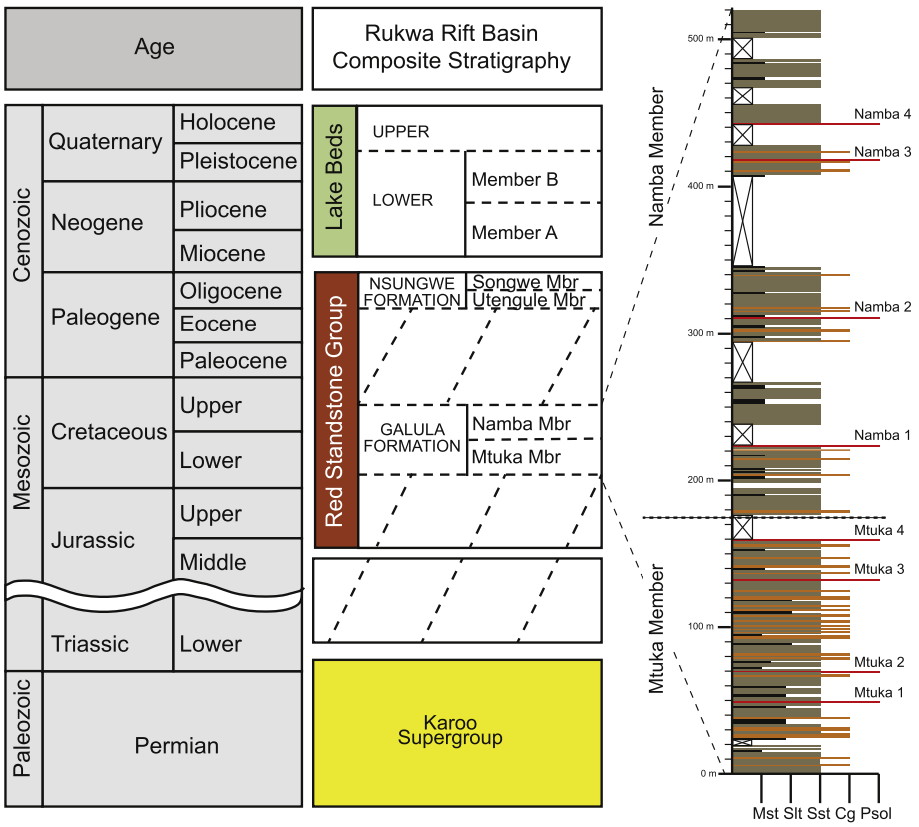

Fig. 2. Composite stratigraphy for the Rukwa Rift Basin and stratotype section for the Galula Formation along the Mtuka River (modified after Roberts et al., 2004, 2010) and stratigraphic location of paleosols described in text. Mbr – Member.

Mtuka 2, while PWI values range from 33 to 94, and a mean less than 40 limited to Mtuka 2. $La/Lu_{(N)}$ values greater than 1 indicate acidic weathering conditions for Mtuka 1, 2 and 3; however, more acidic and reducing conditions in Mtuka 2 is evidenced by negative ΣREE and positive Eu/Eu* deviations from parent material (Table 2). A $La/Lu_{(N)}$ value less than 1 indicates alkaline conditions dominated at the time Mtuka 4 formed.

The Mtuka paleosols experienced moderate calcification, with CAL values ranging from 0.9–4.9. Mtuka 1, 3 and 4 are considered calcareous with CAL values greater than the threshold (CAL > 2) defined by Retallack (1997), although calcification is less evident in the non-Bk horizons of Mtuka 3 and 4. Mtuka 2 is not regarded as calcareous, with CAL values in all horizons less than 2. Application of the clayeyness ratio suggests all units are sandy soils, with low clay production during pedogenesis. Deviation from parent material is minimal (< 0.03) in Mtuka 1, 3 and 4, with Mtuka 2 exhibiting greater clay production with a deviation from parent of 0.1. Clayeyness ratio increases in Bt-horizons confirmed the field classifications, except Mtuka 4, which reported a negative deviation from its parent material and suggests the influence of surface leaching. Hydrolysis values were below 2, as is typical of most soils, especially those with high base status, such as Argillisols (e.g. Mtuka 2), or the modern equivalent, Alfisols. Ba/Sr values range from 0.5–4.6 and indicate leaching (Ba/Sr > 2; Retallack, 1997) at all sites, excluding Mtuka 1. Ratio increases down profile in Mtuka 2 and 3 represent subsurface leaching, whereas Mtuka 4 underwent surface leaching, with the highest Ba/Sr ratio (4.6) recorded near the top of the profile. Oxidation ratios are moderate (0.2–0.6), with little variation down profile. Salinization is minimal, with low SAL values (SAL < 0.3) and no observable increases up profile in all units.

A nearly constant Ti/Al ratio in all paleosols provides evidence for a common provenance. Ti/Al values vary from 0.06 to 0.16, with a mean of 0.10. A number of other trace element ratios are also consistent for all four units (Fig. S1).

Stable isotopic composition of pedogenic carbonates indicate that $\delta^{18}O_{CaCO3}$ values ranged from −4.1 to −6.6‰ (μ = -5.5‰, σ = 0.6‰, n = 43) for the Mtuka Member (Table 3). Mtuka 1 and 2 recorded similar mean $\delta^{18}O$ values of −5.9‰ and − 6.0‰, respectively. The $\delta^{18}O$ values increase up section, with means of −5.5‰ and − 4.7‰ determined for Mtuka 3 and 4.

4.2. Namba Member

4.2.1. Macromorphology

Four paleosols (Namba 1–4) were identified and described from the Namba Member (for detailed descriptions see Supplementary Materials online). The paleosols are hosted in deep red (2.5YR and 10R 3/6–4/8), fine- to medium-grained, well-sorted subarkosic to lithic arkosic sandstones and stratigraphically located between red to purple tabular sandstone units (Fig. 2). Purple trough cross-bedded sandstones frequently incise into the upper horizons of the profiles. The Namba 1 and 2 paleosols are complex soil successions. Namba 1 is a compound paleosol, composed of a lower composite profile (1B) and an upper simple profile (1A), while Namba 2 is a composite paleosol with extensive B-horizon overprinting. Namba 3 and 4 are single isolated, simple profiles (Fig. 3). Each of the Namba paleosols has been incised and truncated, with no evidence of an A-horizon remaining. Soil structure is predominantly angular blocky, with occasional sub-angular blocky fabric also observed (Table 4). Horizonation is well developed in each of the simple, composite and compound paleosol profiles, with thin horizons frequent in the more complex profiles (Table 4). Vertic features are minimal, with slickensides limited to Namba 1 and 4. Pedogenic carbonate accumulations are typically filamentous (stage I) to nodular (0.5–3 cm; stage II) in most profiles, with rare instances of coalesced nodules (stage III) (Fig. 6). Carbonate accumulations were not

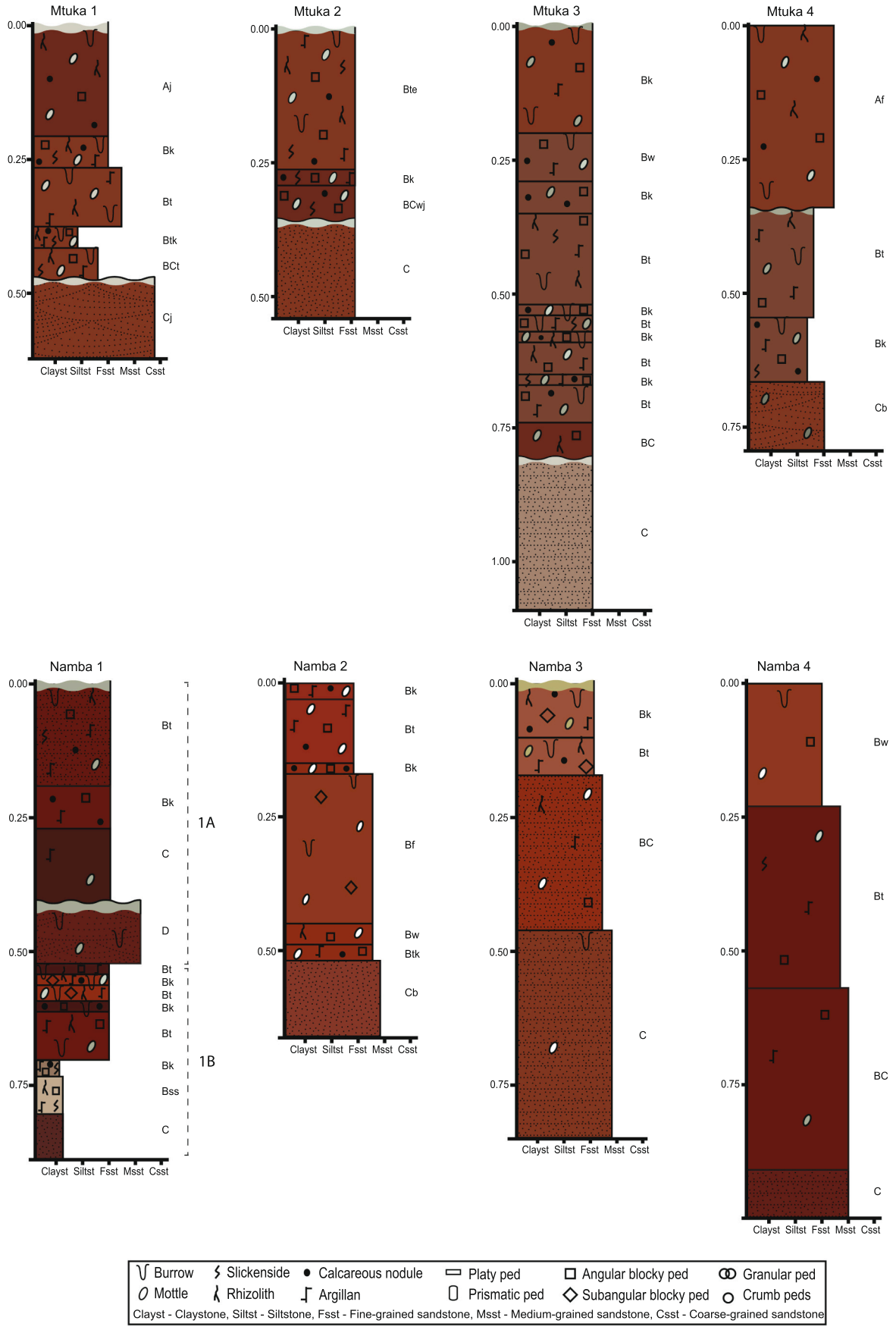

Fig. 3. Detailed measured sections and pedogenic features of Mtuka and Namba paleosols. Matrix and mottle colors are based on Munsell colors, as determined in the field (Refer to Supplementary data for Munsell colour characterization of each horizon) See Fig. 2 for stratigraphic positions.

Table 1
Morphological features of the Galula Formation, Mtuka Member paleosols according to horizon.

Paleosol	Horizon	Depth	Horizon boundaries		Ped		$CaCO_3$ nodules	Bioturbation
		(m)	Sharpness	Lateral continuity	Structure	Size class		
Mtuka 4	Af	0.00–0.35	Abrupt	Wavy	Angular blocky	Medium	Common	Root casts & surface constrained burrows
	Bt	0.35–0.54	Clear	Smooth	Wedge-shaped to angular blocky	Medium	–	Root casts & non-constrained burrows
	Bk	0.54–0.64	Clear	Wavy	Wedge-shaped	Medium	Abundant	Non-constrained burrows
	C	0.64–0.74+	Gradual	Wavy	–	–	–	–
Mtuka 3	Bk	0.00–0.20	Clear	Wavy	Angular blocky	Very coarse	Common	Surface constrained burrows
	Bw	0.20–0.29	Gradual	Smooth	Angular blocky	Coarse	Few	Surface constrained burrows
	Bk	0.29–0.35	Clear	Wavy	Angular blocky	Coarse	Common	–
	Bt	0.35–0.52	Clear	Smooth	Angular blocky	Coarse	–	Root molds & non-constrained burrows
	Bk	0.52–0.54	Clear	Smooth	Angular blocky	Coarse	Common	Non-constrained burrows
	Bt	0.54–0.57	Clear	Smooth	Angular blocky	Coarse	–	Non-constrained burrows
	Bk	0.57–0.59	Clear	Smooth	Angular blocky	Coarse	Common	Root molds & non-constrained burrows
	Bt	0.59–0.65	Clear	Smooth	Angular blocky	Coarse	–	Root molds & non-constrained burrows
	Bk	0.65–0.67	Clear	Smooth	Angular blocky	Coarse	Common	Root casts & non-constrained burrows
	Bt	0.67–0.74	Clear	Smooth	Angular blocky	Coarse	Rare	Root casts & non-constrained burrows
	BC	0.74–0.81	Clear	Smooth	Angular blocky	Coarse	–	Root casts
	C	0.81–1.10	Gradual	Wavy	–	–	–	–
Mtuka 2	Bte	0.00–0.26	Clear	Wavy	Angular blocky to crumb	Fine	Common	Root casts & non-constrained burrows
	Bk	0.26–0.29	Clear	Wavy	Angular blocky	Medium	Abundant	–
	BCwj	0.29–0.3	Clear	Irregular	Angular blocky	Coarse	Few	–
	C	0.36–0.54	Clear	Wavy	–	–	–	–
Mtuka 1	Aj	0.00–0.21	Gradual	Irregular	Angular blocky to prismatic	Coarse	Few to Common	Root casts, rhizohaloes, rhizocretions & weakly defined burrows
	Bk	0.21–0.27	Clear	Smooth	Angular blocky to prismatic	Medium	Abundant	Root casts, rhizohaloes, rhizocretions & weakly defined burrows
	Bt	0.27–0.38	Gradual	Irregular	Angular blocky	Medium	–	Root casts, rhizohaloes, rhizocretions & non-constrained defined burrows
	Btk	0.38–0.42	Clear	Wavy	Angular blocky	Medium	Common	Root casts, rhizohaloes, rhizocretions & non-constrained defined burrows
	BCt	0.42–0.48	Clear	Wavy	Angular blocky	Medium	–	Root casts, rhizohaloes, rhizocretions & weakly defined burrows
	Cj	0.48–0.63	Clear	Wavy	–	–	–	–

observed in Namba 4. The profiles contain evidence of bioturbation, including sediment infilled burrows (meniscate and unlined) and rhizoliths; narrow root casts with calcium carbonate accumulation are the most common forms of root traces observed (Fig. 6; Table 4). Many burrows, root traces and pedogenic nodules are surrounded by white to olive-green haloes. Fe-oxide staining was also observed along the root casts and ped planes of Namba 3 (Fig. 6A-B). The Namba paleosols are predominantly argillic, with abundant illuvial clay features and common calcic accumulations, classifying Namba 1 and 2 as calcic Argillisols, and Namba 3 as an argillic Calcisol. Namba 4 exhibited only weak pedogenesis, and as such, represents an argillic Protosol.

4.2.2. *Micromorphology*

Examination of thin sections revealed a fine-grained matrix, with angular to sub-angular blocky fabric for all four Namba paleosols (Fig. 6I). The coarse fraction is composed principally of quartz with minor feldspars and lithic fragments, and trace heavy minerals (Fig. 6I-K). Evidence of bioturbation was limited to root fines, which were not observed in the Namba 4 thin section. Mottling and clear areas of oxidized and reduced mudstone are limited to Namba 1 and 2, whereas Namba 4 is notably clay-rich, with abundant desiccation features (Fig. 6I-L). Pervasive filamentous and nodular calcium carbonate accumulations were observed in the thin sections of Namba 2 and 3 (Fig. 6J).

4.2.3. *Composition*

The clay mineralogy is dominated by montmorillonite (70–83%) and illite (15–30%), with minor proportions of kaolinite (1–2%) limited to Namba 1 and 3. There was no observable variation between the different paleosol types (i.e. calcic Argillisol and argillic Calcisol).

Weathering ratio results for the Namba paleosols are provided in Fig. 7. The CIA and PWI identify moderate weathering in Namba 1, 2 and 4 and incipient to weak weathering and pedogenesis in Namba 3. CIA values range from 30 to 79, with a mean less than 50 limited to Namba 3, while PWI values range from 32 to 77, and a mean greater than 50 limited to Namba 3. $La/Lu_{(N)}$ values less than 1 indicate neutral to alkaline weathering conditions for all Namba paleosols; however, $La/Lu_{(N)}$ values for Namba 1 and 4 are 0.9, and negative ΣREE and positive Eu/Eu* deviations from parent indicate Namba 1 and 4 formed under acidic and reducing conditions (Table 2). A positive Ce anomaly relative to parent confirms alkaline conditions for Namba 2.

The Namba paleosols experienced low to moderate calcification during pedogenesis, with CAL values ranging from 0.7 to 3.0. Namba 3 is moderately calcareous with CAL > 2, whereas Namba 1 and 2 are less calcareous, with CAL values greater than 2 limited to the Bk-horizons. Namba 4 is non-calcareous, with CAL < 1. The clayeyness ratio identifies all units as sandy soils, with low clay production during pedogenesis. Deviation from parent is indistinguishable in Namba 2, with minimal deviation observed in Namba 3 (< 0.03). Namba 1 and 4 exhibit moderate clay production with a deviation from parent material of > 0.04 and clayeyness ratio increases in the field classified Bt-horizons. Hydrolysis values are below 2, as is typical of most soils. However, hydrolysis ratio increases down profile suggest Namba 1 and 2 underwent subsurface weathering, whereas increased ratio values towards the top of the profile suggests surface weathering in Namba 4. Ba/Sr values are less than 1 in all units except Namba 1 (1.4–4.9), and indicate leaching was limited to Namba 1. Namba 1 is a compound paleosol and ratio changes down profile suggest leaching varied between the soils, with surface leaching evident in the upper unit and subsurface leaching in the lower. Low OX values (0.2–0.4) indicate weak oxidation and a steady climate in all units, with any down profile

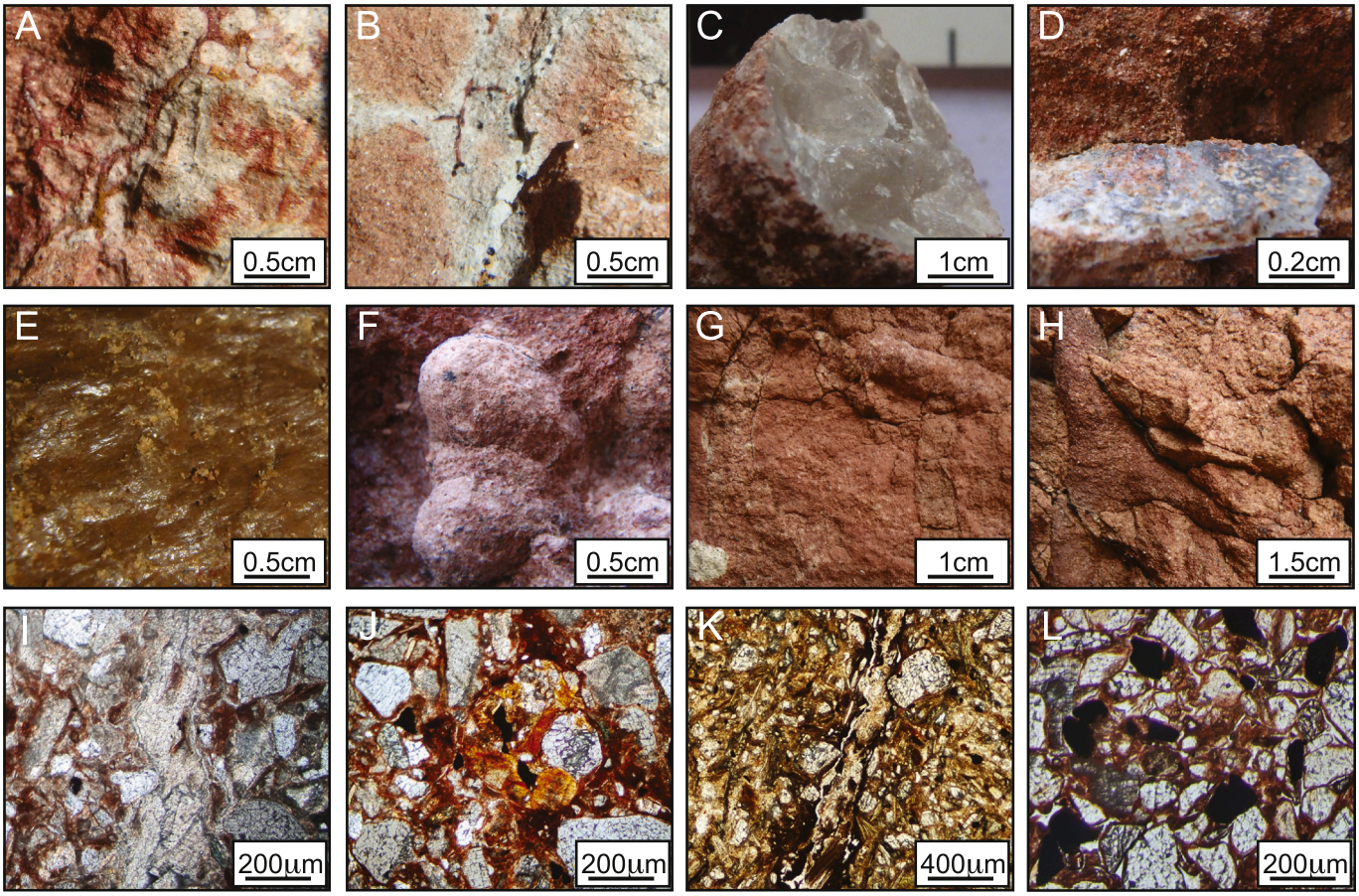

Fig. 4. A–B: Clay lined rhizoliths with calcium carbonate and hematite accumulations (Mtuka 1); C: Calcium carbonate replaced rhizocast (Mtuka 1); D: Calcium carbonate replaced rhizocast (Mtuka 3); E: Slickensides (Mtuka 4); F: Pedogenic carbonate nodules (Mtuka 3); G–H: Sediment filled burrows (Mtuka 4); I: Calcium carbonate replaced rhizolith (10× cross-polarized light; Mtuka 1); J: Clay, detrital Fe-oxide grains and siderite accumulation (10× cross-polarized light; Mtuka 2); K: Fe-oxide along root channel (4× plane-polarized light; Mtuka 3); L: Quartz dominated coarse-fraction and detrital Fe-Ti oxide grains surrounded by clay (10× cross-polarized light; Mtuka 4).

changes minimal and limited to Namba 1 and 2. Salinization is also minimal, with SAL values less than 0.4 in all units, and well below the salinization threshold (SAL > 2).

A consistent Ti/Al ratio in all Namba paleosols provides evidence for a common provenance. Ti/Al values vary from 0.08 to 0.19, with a mean of 0.10. Several other trace element ratios are also nearly constant for all 4 units (Fig. S1).

$\delta^{18}O_{CaCO3}$ values for Namba paleosols range from −6.2 to −7.8‰ (μ = -7.2‰, σ = 0.5‰, n = 20) for paleosols Namba 1 to 3 (Table 3); although notably, Namba 4 did not contain pedogenic carbonate nodules. A mean $\delta^{18}O$ value of −6.7‰ was recorded for Namba 1, with more negative values recorded for Namba 2 (μ = −7.7‰) and Namba 3 (μ = −7.4‰).

5. Discussion

5.1. Paleoclimate

5.1.1. Mtuka Member

Paleoprecipitation (MAP) estimates for the Mtuka Member average 710 mm/yr, with various MAP proxies indicating MAP values of 436 ± 141 mm/yr (DTC), 540 ± 108 mm/yr (CALMAG), 760 ± 181 mm/yr (CIA—K), and 968 ± 228 mm/yr (PPM1.0). The PPM1.0 and geochemical proxy (CIA-K and CALMAG) derived MAP estimates exhibit moderate ranges, whereas DTC derived MAP values estimate both a narrow range and the lowest values. However, the DTC proxy was only applied to Mtuka 1 and 4, as the relationship is only relevant for profiles that are not truncated. It is however never possible to guarantee that a particular unit is preserved in its entirety (Miall, 2015). Mtuka 1 and 4 exhibit wavy to irregular upper boundaries, and are overlain by fluvial deposits, suggesting that part of the soil was likely eroded and that DTC-MAP values are somewhat underestimated. The MAP values for Mtuka paleosols 1, 2, 3 and 4 are 454 mm/yr, 731 mm/yr, 833 mm/yr and 860 mm/yr respectively (Fig. 8), and mostly fall within the 2-σ uncertainty range. However, PPM1.0 generated values for Mtuka 1 and Mtuka 4 do not, and may be anomalously high.

Paleotemperature (MAT) estimates for Mtuka paleosols show an average of 13.3 °C. MAT values calculated using major-element paleothermometers (PWI and SAL proxies) range from 10.2 °C to 14.1 °C, whereas non-linear spline model, PPM1.0, determined a slightly larger range in MAT, estimating values of 12.9 °C to 17.2 °C. Carbonate $\delta^{18}O$ values estimate a narrow MAT range of 14.0 °C to 15.6 °C. Average MAT values of 13.5 °C, 13.1 °C, 13.9 °C and 12.9 °C were estimated for Mtuka 1, 2, 3 and 4 respectively (Fig. 8), with Mtuka 3 recording the highest temperature. MAT values for each individual paleosol fall within the 2-σ uncertainty range, indicating that it is highly likely (approximately 95% confidence) that measurements, although obtained from different proxies, are the same for each unit.

The Koppen aridity index (MAP/MAT+33) revealed that, with the exception of Mtuka 1, the paleosols developed in a sub-humid climate; Mtuka 1 is classified as semi-arid. This is in agreement with classification by MAP alone, with Mtuka paleosols 2, 3 and 4 recording sub-humid

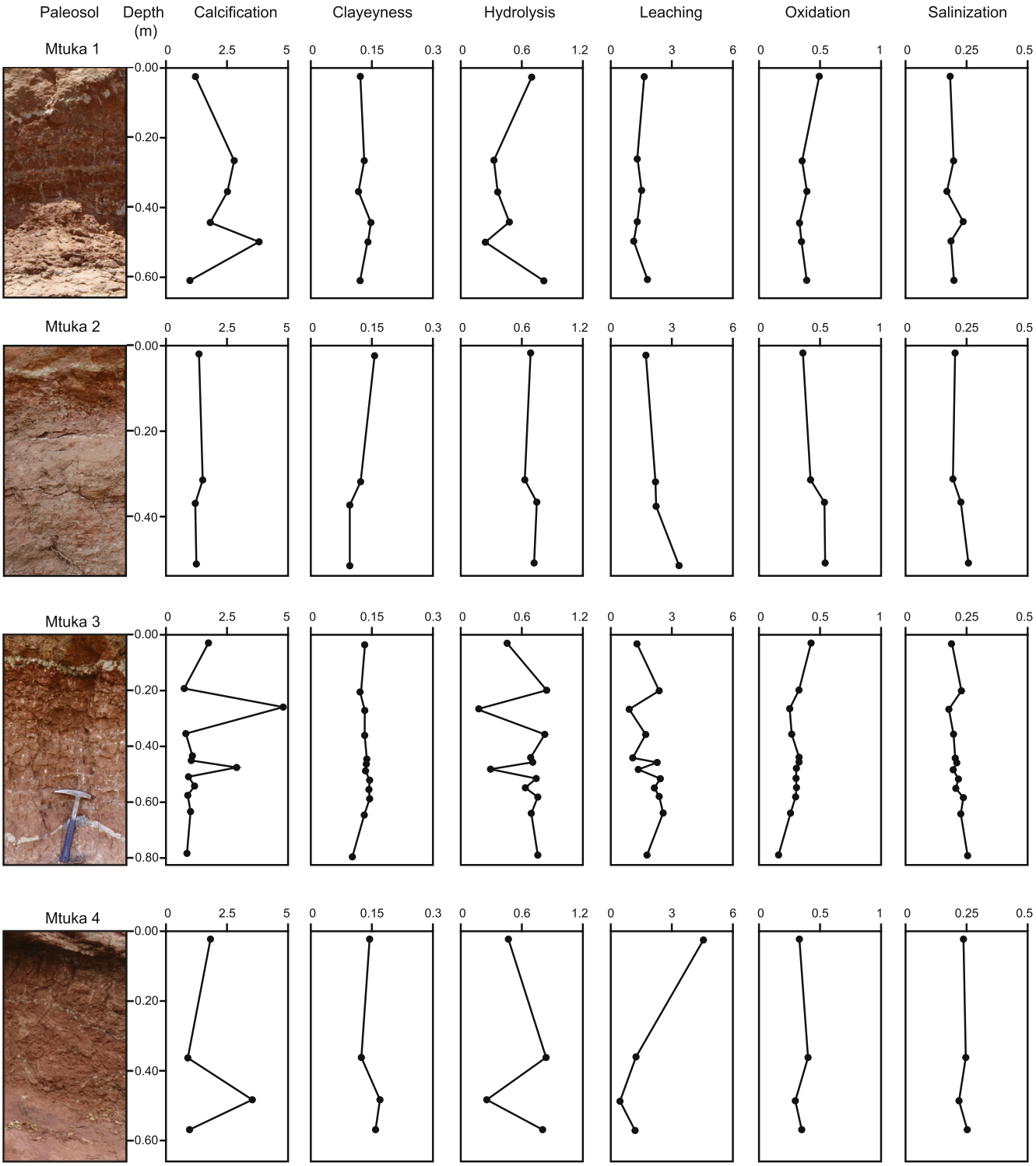

Fig. 5. Mtuka paleosols, showing soil depth and horizons, and selected geochemical weathering ratios. Calcification – $(CaO + MgO)/Al_2O_3$; Clayeyness – Al_2O_3/SiO_2; Hydrolysis - $Al_2O_3/(CaO + MgO + K_2O + Na_2O)$; Leaching – Ba/Sr; Oxidation – Fe_2O_3/Al_2O_3; Salinization – $(K_2O + Na_2O)/Al_2O_3$).

rainfall (500 mm < MAP <1000 mm; Bull, 1991), and Mtuka 1 falling within the semi-arid range (250 mm < MAP <500 mm; Bull, 1991). Paleoclimatic implications of clay mineralogy are less clear. The presence of palygorskite is indicative of arid to semi-arid conditions, where evaporation exceeds precipitation (da Silva et al., 2017, 2018). Indeed, palygorskite becomes unstable in soils that experience precipitation >300 mm/yr (Paquet and Millot, 1972; da Silva et al., 2018; Delgado et al., 2019), an amount far lower than any of the estimated MAP values. Yet palygorskite has also been recorded in paleosols that exhibit argillic features (e.g. Nettleton and Peterson, 1983; Khademi and Mermut, 1999; Khormali and Abtahi, 2003; da Silva et al., 2018; Varela et al., 2018). Khademi and Mermut (1999) interpret this coexistence as evidence for dry conditions interspersed with pluvial periods. Certainly, the presence of beidellite and pedogenic calcite supports a climate of wet and dry alternations (Alekseeva et al., 2018).

Overall, the Mtuka paleosols demonstrate moderate seasonality of

Table 2
Rare earth element data for the Mtuka and Namba paleosols and their associated parent material.

Paleosol	ΣREE	Eu/Eu*	$La/Lu_{(N)}$
Namba 4	213	1.1	0.9
Parent - Namba 4	374	0.8	0.9
Namba 3	187	1.2	0.9
Parent - Namba 3	169	1.2	0.6
Namba 2	192	1.0	0.7
Parent - Namba 2	103	1.3	0.7
Namba 1	180	1.1	0.9
Parent - Namba 1	321	1.1	0.8
Mtuka 4	210	1.1	0.9
Parent - Mtuka 4	166	1.1	0.9
Mtuka 3	158	1.3	1.1
Parent - Mtuka 3	99	1.3	1.0
Mtuka 2	179	1.2	1.2
Parent - Mtuka 2	224	1.0	1.1
Mtuka 1	145	1.3	1.0
Parent - Mtuka 1	134	1.3	1.0

Table 3
Stable oxygen isotope composition of pedogenic carbonates from the Mtuka and Namba paleosols.

Paleosol	$\delta^{18}O$ $CaCO_3$ (‰ VPDB)	Mean (‰)	1σ (‰)	n
Namba 4	–	–	–	–
Namba 3	−7.2 to −7.4	−7.4	0.1	4
Namba 2	−7.4 to −7.8	−7.7	0.2	6
Namba 1	−6.2 to −7.4	−6.7	0.4	10
Mtuka 4	−4.1 to −5.6	−4.7	0.5	11
Mtuka 3	−5.4 to −5.6	−5.5	0.1	8
Mtuka 2	−5.6 to −6.6	−6.0	0.3	10
Mtuka 1	−5.6 to −6.4	−5.9	0.2	10

precipitation, with a mean annual range of 39 mm/yr to 71 mm/yr. A seasonal climate for the Mtuka was also suggested by Roberts et al. (2010), with armoured mudballs and ubiquitous mud rip-up clasts observed throughout the stratotype suggestive of flashy fluvial discharge in the paleochannels. This is further supported by a number of morphological characteristics. Grey-green mottles and rhizohaloes indicate enough rainfall for Fe depletion, but typically insufficient for hematite accumulation along the edges of the rhizoliths (Kraus and Hasiotis, 2006). Moderate oxidation ratios attest to sufficient saturation for Fe mobilization during wet periods, but also of the fixation of Fe oxides during drying (Ashley and Driese, 2000; Driese et al., 2016). The presence of argillans indicates rainfall sufficiently ample for downward translocation of clays, with vertic features and angular blocky to wedge-shaped peds evidence that pedogenesis was dominated by the shrinking and swelling of such clays during wet and dry periods (Birkeland, 1999). Accumulations of stage I-IV pedogenic carbonates also indicate sufficient aridity for precipitation of calcium carbonate, with calcareous rhizocretions further evidence for episodic drying (Kraus and Hasiotis, 2006). Traditionally, pedogenic carbonates have been interpreted to indicate aridity (e.g. Tabor and Myers, 2015), but recent studies suggest they may also suggest pronounced seasonality (Aslan and Autin, 1998; Tabor and Myers, 2015), with carbonates forming in the warmest months immediately preceding periods of heavy rainfall (Breecker et al., 2009; Burgener et al., 2019). Thick and diffuse Bk horizons also imply seasonal rainfall (Retallack, 2005).

The prevalence of vertic Calcisols suggests that semi-arid to sub-humid and seasonal climates prevailed throughout pedogenesis of the Mtuka paleosols. Calcisols and Vertisols typically occur in the dry subtropics, where the principal pedogenic process is accumulation of calcium carbonate, with seasonal rainfall favouring vertic features and some gley characteristics (Mack and James, 1994). Indeed, weathering ratios highlight calcification as the dominant pedogenic process in all units, excluding Mtuka 2. Mtuka 2 is clay-dominated and the only vertic Argillisol of the studied Mtuka units.

5.1.2. Namba Member

Paleoprecipitation climofunctions estimate an average MAP of 767 mm/yr for Namba Member paleosols, with MAP values of 643 ± 108 mm/yr (CALMAG), 697 ± 181 mm/yr (CIA-K), and 901 ± 228 mm/yr (PPM1.0) determined by different proxies. PPM1.0 estimates displayed the greatest range and highest MAP values, with geochemical proxies (CIA-K and CALMAG) exhibiting a smaller range. MAP values for Namba paleosols 1, 2, 3 and 4 are 683 mm/yr, 730 mm/yr, 602 mm/yr and 987 mm/yr, respectively (Fig. 8). Values for each individual paleosol, excluding Namba 4, fall within the 2-σ uncertainty range, and are not statistically different. PPM1.0 values for Namba 4 fall outside the 2-σ uncertainty range and are likely an overestimation.

Paleotemperatures (MAT) averaged 11.9 °C for the Namba paleosols, with a range of 8.7 °C to 14.3 °C. The PPM1.0 model displays the largest range in MAT values with estimates of 8.7 °C to 14.3 °C, whereas major-element paleothermometers (PWI and SAL proxies) calculate a slightly smaller range of 9.7 °C to 12.8 °C. Carbonate derived $\delta^{18}O$ data determine a narrow MAT range of 12.0 °C to 13.1 °C for Namba paleosols, excluding Namba 4 which lacked pedogenic carbonates. Average MAT values of 12.5 °C, 12.0 °C, 12.3 °C and 10.3 °C were estimated for Namba 1, 2, 3 and 4, respectively (Fig. 8), with Namba 4 recording the lowest temperature. MAT values for each individual paleosol fall within the 2-σ uncertainty range, indicating that it is highly likely (approximately 95% confidence) that measurements are the same for each paleosol.

The Koppen aridity index determined Namba paleosols formed in a sub-humid climate, excluding Namba 4, which developed in a humid climate. This is broadly in agreement with classification by MAP alone, with all Namba paleosols recording sub-humid rainfall (500 mm < MAP <1000 mm; Bull, 1991). Namba 4 fell slightly outside the humid range (1000 mm < MAP <2000 mm; Bull, 1991), with a MAP value of 987 mm/yr. Dominance of smectite (montmorillonite) also indicates a sub-humid climate, with modern soils of similar clay compositions observed in parts of the sub-humid Mediterranean (Tabor et al., 2004).

Namba paleosols exhibit weak seasonality of precipitation, recording a difference of just 29 mm/yr to 39 mm/yr between the wettest and driest months. Macromorphological features also suggest a consistently wet climate, with weak seasonality. Presence of thin, concentrated Bk horizons suggests little seasonality (Retallack, 2005), with illuviation of clays, various argillic phases, and development of thick Bt horizons all indicating a wet climate (Ashley and Driese, 2000). Grey-green rhizohaloes with yellow-brown Fe-oxide accumulations are the product of sufficiently wet and anoxic soils, reducing and mobilizing Fe towards areas of oxidation along the root channels of the paleosols (Kraus and Hasiotis, 2006). Yellow-brown staining likely indicates goethite, which typically accumulates in wetter soils than hematite-hosting soils (e.g. PiPujol and Buurman, 1997; Kraus and Hasiotis, 2006), such as Mtuka 1.

The presence and accumulation of pedogenic carbonates, and stage II carbonates in particular, implies occurrence of some dry periods (Aslan and Autin, 1998; Kraus and Riggins, 2007) in the Namba Member. However, calcium carbonate accumulations in Namba units are predominantly filamentous (stage I), and are absent entirely from Namba 4. Excluding Namba 3, stage II nodular accumulations are small (~0.5 cm in diameter), with larger accumulations (~1–3 cm in diameter) in Namba 3 illustrating its classification as the sole Calcisol of studied units in the Namba Member. Furthermore, although pedogenic carbonates are typically associated with aridity and more common in soils with a MAP of < 600 mm (Mack and James, 1992), they are also found in soils with a MAP up to 1000 mm (Nordt et al., 2006). Overall, weakly developed carbonates suggest aridity and calcium carbonate precipitation were not dominant pedogenic drivers.

Taxonomic classification as Argillisols, or at least subordinately argillic paleosols, suggests that Namba soils formed under moderate to high annual rainfall, with illuviation of clay as a dominant pedogenic

Table 4
Morphological features of the Galula Formation, Namba Member paleosols according to horizon.

Paleosol	Horizon	Depth	Horizon boundaries		Ped		$CaCO_3$ nodules	Bioturbation
		(m)	Sharpness	Lateral continuity	Structure	Size class		
Namba 4	Bw	0.00–0.23	Abrupt	Smooth	Angular blocky	Coarse	–	Surface constrained burrows
	Bt	0.23–0.57	Clear	Wavy	Angular blocky	Very Coarse	–	–
	BC	0.57–0.91	Clear	Smooth	Angular blocky	Very Coarse	–	–
	C	0.91–0.97	Clear	Smooth	–	–	–	–
Namba 3	Bk	0.00–0.10	Abrupt	Wavy	Subangular blocky	Medium	Abundant	Root casts, root tubules & surface constrained meniscate burrows
	Bt	0.10–0.17	Gradual	Smooth	Subangular blocky	Medium	Few	Root casts, root tubules & surface constrained meniscate burrows
	BC	0.17–0.46	Gradual	Smooth	Angular blocky	Very Coarse	–	–
	C	0.46–0.86	Gradual	Smooth	–	–	–	–
Namba 2	Bk	0.00–0.03	Abrupt	Irregular	Angular blocky	Coarse	Abundant	–
	Bt	0.03–0.15	Clear	Smooth	Angular blocky	Very Coarse	Few	–
	Bk	0.15–0.17	Clear	Irregular	Angular blocky	Coarse	Abundant	–
	Bf	0.17–0.45	Clear	Smooth	Subangular blocky	Very Coarse	–	Non-constrained burrows
	Bw	0.45–0.49	Clear	Smooth	Angular blocky	Very Coarse	–	Root casts
	Btk	0.49–0.52	Clear	Irregular	Angular blocky	Coarse	Abundant	–
	C	>0.52	Clear	Irregular	–	–	–	–
Namba 1	Bt	0.00–0.19	Clear	Wavy	Angular blocky	Coarse	Common	Root casts & non-constrained burrows
(1A)	Bk	0.19–0.27	Clear	Wavy	Angular blocky	Coarse	Abundant	–
	C	0.27–0.41	Clear	Irregular	–	–	–	–
	D	0.41–0.52	Clear	Wavy	–	–	–	–
(1B)	Bt	0.52–0.54	Clear	Smooth	Angular blocky	Coarse	–	Root casts & non-constrained burrows
	Bk	0.54–0.56	Clear	Smooth	Subangular blocky	Coarse	Abundant	Root casts & root tubules
	Bt	0.56–0.59	Clear	Smooth	Subangular blocky	Coarse	Few	Root casts & non-constrained burrows
	Bk	0.59–0.61	Clear	Smooth	Angular blocky	Coarse	Abundant	Root casts & non-constrained burrows
	Bt	0.61–0.70	Clear	Smooth	Angular blocky	Coarse	–	Non-constrained burrows
	Bk	0.70–0.72	Clear	Smooth	Angular blocky	Medium	Abundant	Non-constrained burrows & root casts
	Bss	0.72–0.79	Gradual	Wavy	Angular blocky	Medium	–	Root casts & root tubules
	C	>0.79	Clear	Smooth	–	–	–	–

process (Mack and James, 1994). Indeed, according to the United States Natural Resources Conservation (1999), modern equivalents of low base Argillisols, 'Ultisols', and high base Argillisols, 'Alfisols', form in climatic conditions of almost any soil temperature and any soil moisture, excluding aridic. Weathering ratio calculations also indicate hydrolysis as the dominant pedogenic process; excluding Namba 3, where calcification dominated.

5.2. Paleoenvironment

5.2.1. Mtuka Member

Mtuka paleosols formed on sub-aerially exposed normally graded fluvial deposits that likely represent an infilled braided channel of a dynamic floodplain. Predominantly simple profiles represent mature soils that formed in periods or areas cut-off from sedimentation (Kraus, 1999). The sole composite profile (Mtuka 3) signifies pedogenesis interrupted by brief, rapid episodes of sedimentation (Marriott and Wright, 1993), likely from the periodic inundation of the floodplain (McCarthy and Plint, 1998).

Angular blocky ped development in all profiles suggests substantial uninterrupted periods of pedogenesis that involved cracking around roots and burrows, and shrinking and swelling during wet and dry periods (Birkeland, 1999). Instances of wedge-shaped peds and slickensides are further evidence of mature soils (e.g. Retallack, 2001; Johnson, 2004 and references therein).

Abundant calcareous root casts, molds, and rhizocretions of Mtuka paleosols indicate moderately well-drained soils. Calcareous rhizoliths are common in moderately well-drained red paleosols (Kraus and Hasiotis, 2006). Whilst grey-green rhizohaloes are the product of gleying, lack of Fe-oxide accumulation along the boundaries of the Fe depletion suggests moderately well-drained soils subjected to moderate surface-water gley processes (Kraus and Hasiotis, 2006). Green mottled burrows also indicate a moderately well-drained soil environment (Hembree and Bowen, 2017). Moderate Ba/Sr ratios provide further evidence that the Mtuka paleosols were moderately to well-drained, with higher values corresponding to well-drained conditions (Thornburg et al., 2019).

5.2.2. Namba Member

Namba paleosols formed on sub-aerially exposed fluvial deposits that likely represent both channel and overbank deposits of a braided floodplain. Namba 1 and 2 are mature soils with complex profiles that recorded the floodplain's ever-changing environment. Conversely, the simple profiles of Namba 3 and 4 are the product of pedogenesis during periods of insignificant erosion and sedimentation within channels. Namba 4 is an immature soil that underwent little pedogenesis before successive erosional and depositional episodes truncated and buried the soil, whereas Namba 3 is a mature soil with well-developed B-horizons. Mature soils commonly form on the distal floodplain, but the lack of finer sediments (silts and clays) suggests that these soils were nearer to the channel belt (Bown and Kraus, 1987).

Profile morphology provides further insight into individual paleoenvironments on the braidplain. Channel migration may be preserved in composite profiles of Namba 1A and Namba 2. Composite soils with

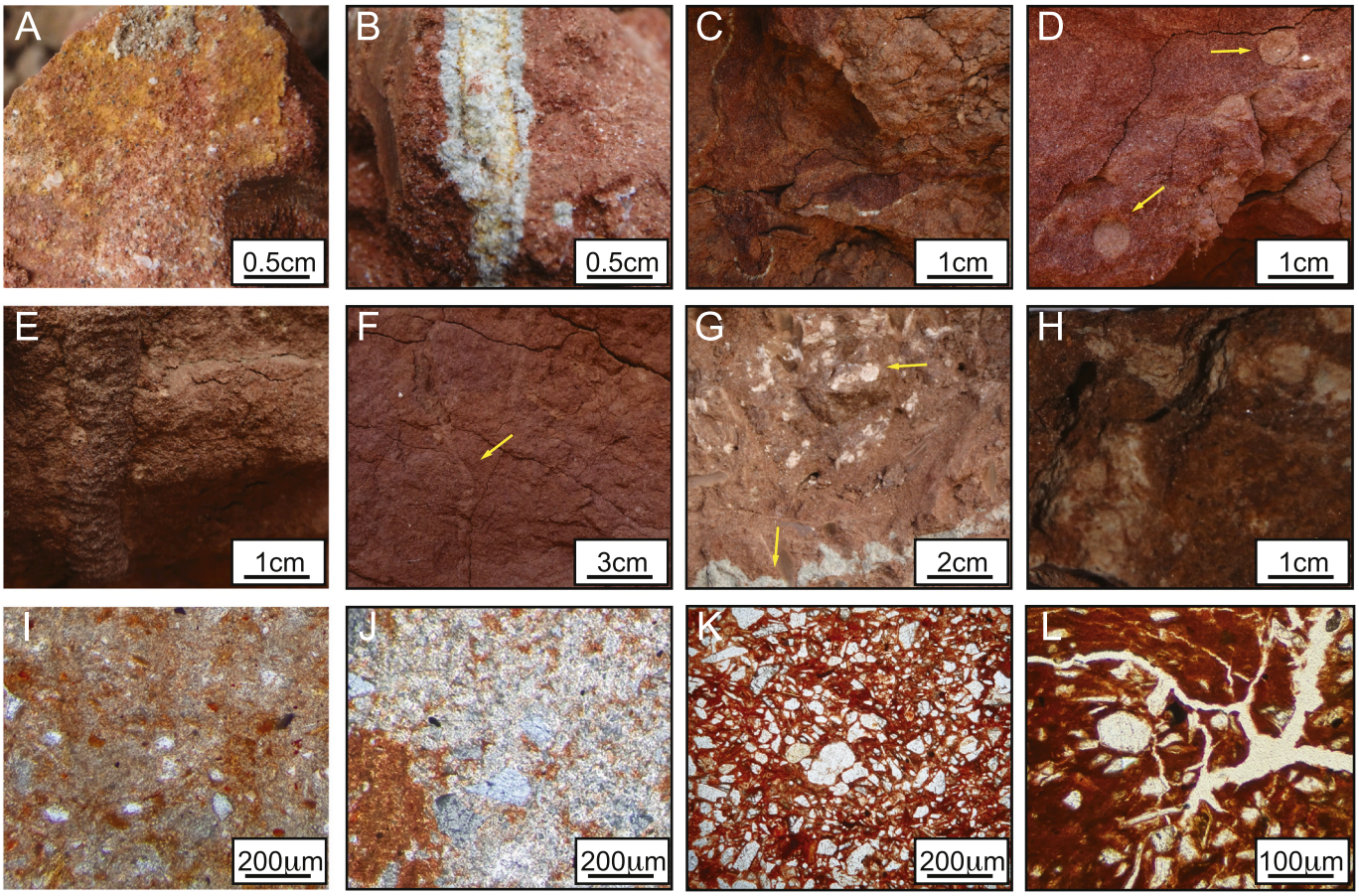

Fig. 6. A: Fe-oxide staining on ped plane (Namba 3); Rhizohalo with Fe-oxide accumulations (Namba 3); C–D: Sediment infilled burrows (Namba 4); E: Meniscate burrow (Namba 3); F: Sediment infilled burrow (Namba 2); G: Pedogenic carbonate accumulation above laterally extensive grey-green mottling (Namba 1); H: Pedogenic carbonate accumulations (Namba 1); I: Mottled fine-grained matrix (10× cross-polarized light; Namba 1); J: Calcium carbonate accumulation (10× cross-polarized light; Namba 2); K: Clay rich matrix with quartz dominated coarse-fraction (10× plane polarized light; Namba 3); L: Clay desiccation features (10× plane polarized light; Namba 4). (For interpretation of the references to colour in this figure legend, the reader is referred to the web version of this article.)

well-developed Bt horizons are thought to form in the upper deposits of laterally migrating channels (Kraus, 1999). Repeated Bt and Bk horizon alternations lacks significant overprinting and suggests that composite soils were indeed proximal to the channel(s), with cumulative profiles more indicative of the distal plain (e.g. Kraus, 1999; Hembree and Hasiotis, 2007). The overall compound profile of Namba 1 (Namba 1A and 1B) is the result of rapid, episodic sedimentation (Marriott and Wright, 1993). Truncation and subsequent burial of stacked soils represents successive erosional and depositional events of sufficient sediment volume to isolate each soil from pedogenesis, and are typical of overbank deposits proximal to active channel(s) (Kraus, 1999; Hamer et al., 2007; Smith et al., 2008). Evidence of intense bioturbation also suggests that compound soils were sub-aerially exposed for an extended period of time between sedimentation events (Therrien et al., 2009).

Bioturbation features in Namba Member paleosols indicate moderately to poorly drained soils. In particular, the unlined, passively filled burrows of Namba 2 and 4 suggest moderately to poorly drained soils, and meniscate burrows of Namba 3 indicate a moderate but moist drainage state (Hembree and Bowen, 2017). Grey-green rhizohaloes observed in all profiles are typical of moderately drained soils, but yellow-brown Fe accumulations at Namba 3 indicate a poorly drained soil (e.g. Kraus and Hasiotis, 2006; Kraus and Riggins, 2007). Indeed, low Ba/Sr ratios suggest that Namba paleosols were poorly drained, excluding Namba 1, which was more moderately drained. In particular, acidic and reducing conditions, common in waterlogged soils (Van Breemen, 1975), are also suggested by the negative ΣREE and positive Eu/Eu* deviations from parent in Namba 1 and 4. Predominance of pedogenic smectite also points to a poorly drained environment (Borchardt, 1989; Sheldon and Tabor, 2009).

5.3. *Paleoclimatic and paleoenvironmental implications for the Galula Formation*

Quantitative analyses of multiple proxies indicate that Galula Formation paleosols formed in a semi-arid to sub-humid climate, with a progressive shift towards wetter conditions through time. This is supported by qualitative observations (e.g. thick Bt horizons, Fe-depletion and Fe-oxide accumulation, gleying, abundant argillic phases and weakly developed carbonate accumulations) that indicate soil development under slightly wetter conditions in the overlying (and younger) Namba Member than for the Mtuka Member. Indeed, pedogenic carbonate accumulations are both more developed and prevalent in Mtuka paleosols, typical of more mature soils (Gile et al., 1966) that formed in arid conditions (Retallack, 2001). Normally, this would also be reflected in a shallower depth to calcic horizon in Mtuka paleosols, relative to Namba paleosols (Retallack, 2005; Hembree and Hasiotis, 2007); however, this is not the case. This disparity is thought to result from Namba paleosols experiencing greater erosional events than those of the Mtuka Member.

Paleosols of the Galula Formation developed predominantly on exposed channel fill deposits across a dynamic, long-lived fluvial braidplain system along the western margin of the NW trending rift

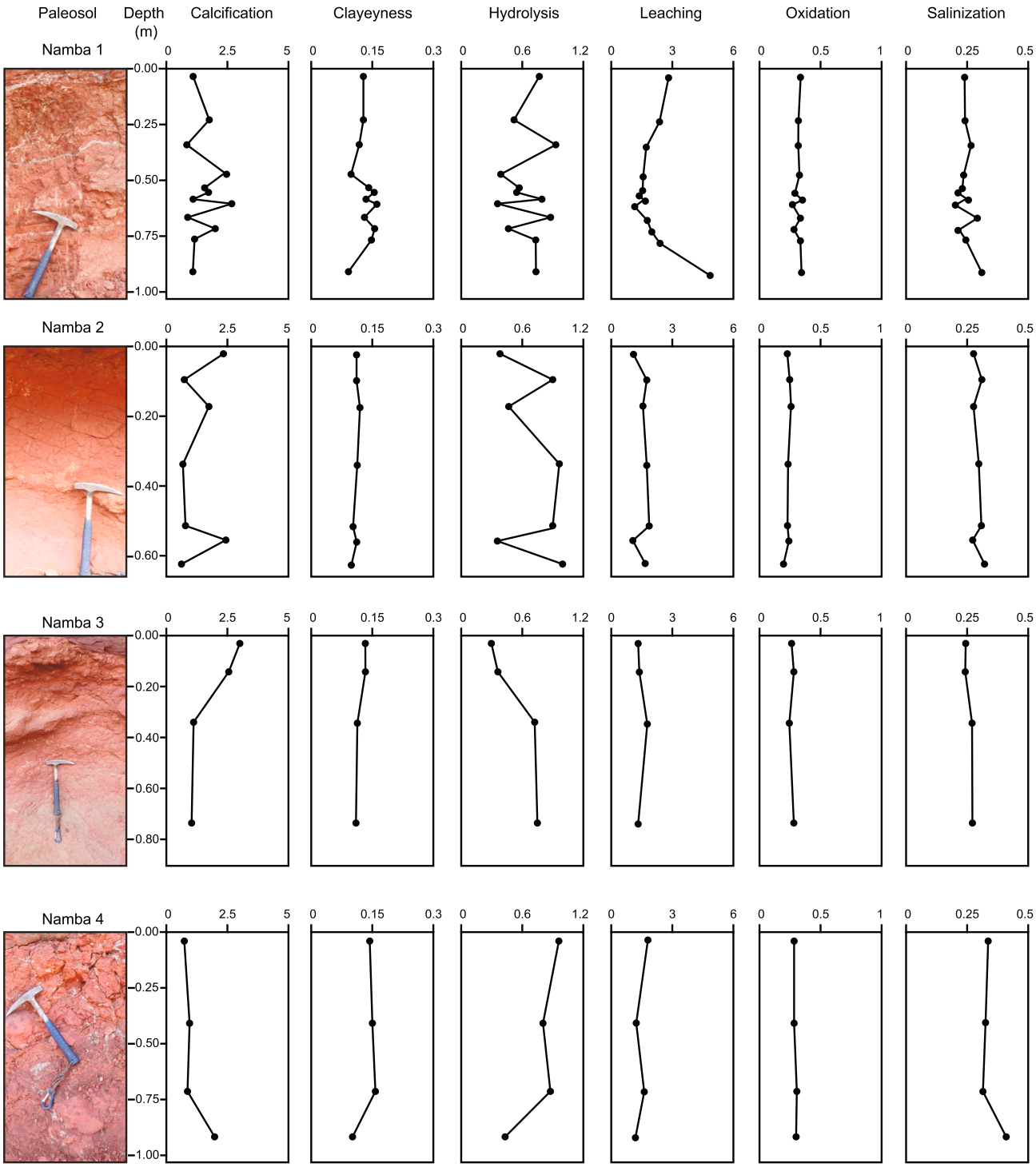

Fig. 7. Namba paleosols, showing soil depth and horizons, and selected geochemical weathering ratios. Calcification – $(CaO + MgO)/Al_2O_3$; Clayeyness – Al_2O_3/SiO_2; Hydrolysis - $Al_2O_3/(CaO + MgO + K_2O + Na_2O)$; Leaching – Ba/Sr; Oxidation – Fe_2O_3/Al_2O_3; Salinization – $(K_2O + Na_2O)/Al_2O_3$).

valley, one that likely extended from northern Malawi to eastern Democratic Republic of Congo along the ~300 km long rift axis (see Roberts et al., 2012). Periodic flooding, sourced from highlands in Malawi and Zambia, led to recruitment and deposition of new sediments in the thin, proximal floodplain deposits represented by both members, with Namba paleosols recording evidence of channel migration or avulsion. This seasonal or cyclical formation, abandonment and in-filling of channels likely provided ideal taphonomic conditions for rapid burial and preservation of vertebrate fossils as well.

Whereas sauropod dinosaurs are the most abundant fossils recovered from the formation to date (e.g. Gorscak et al., 2014, 2017; Gorscak and O'Connor, 2019), the number and diversity of non-dinosaurian taxa recovered from the Galula Formation is significant and highlighted by a range of fully terrestrial and aquatic species. For example, there are currently at least four taxa of notosuchian crocodyliforms (O'Connor et al., 2010; Sertich and O'Connor, 2014), a gondwanatherian mammal (O'Connor et al., 2019), and a number of other terrestrial (e.g. turtles) and freshwater (teleost fish and lungfish) forms recognized (O'Connor et al., 2006; Gottfried et al., 2009), indicative of a diverse, long-lived riverine ecosystem that occupied a semi-arid to sub-humid, low-relief

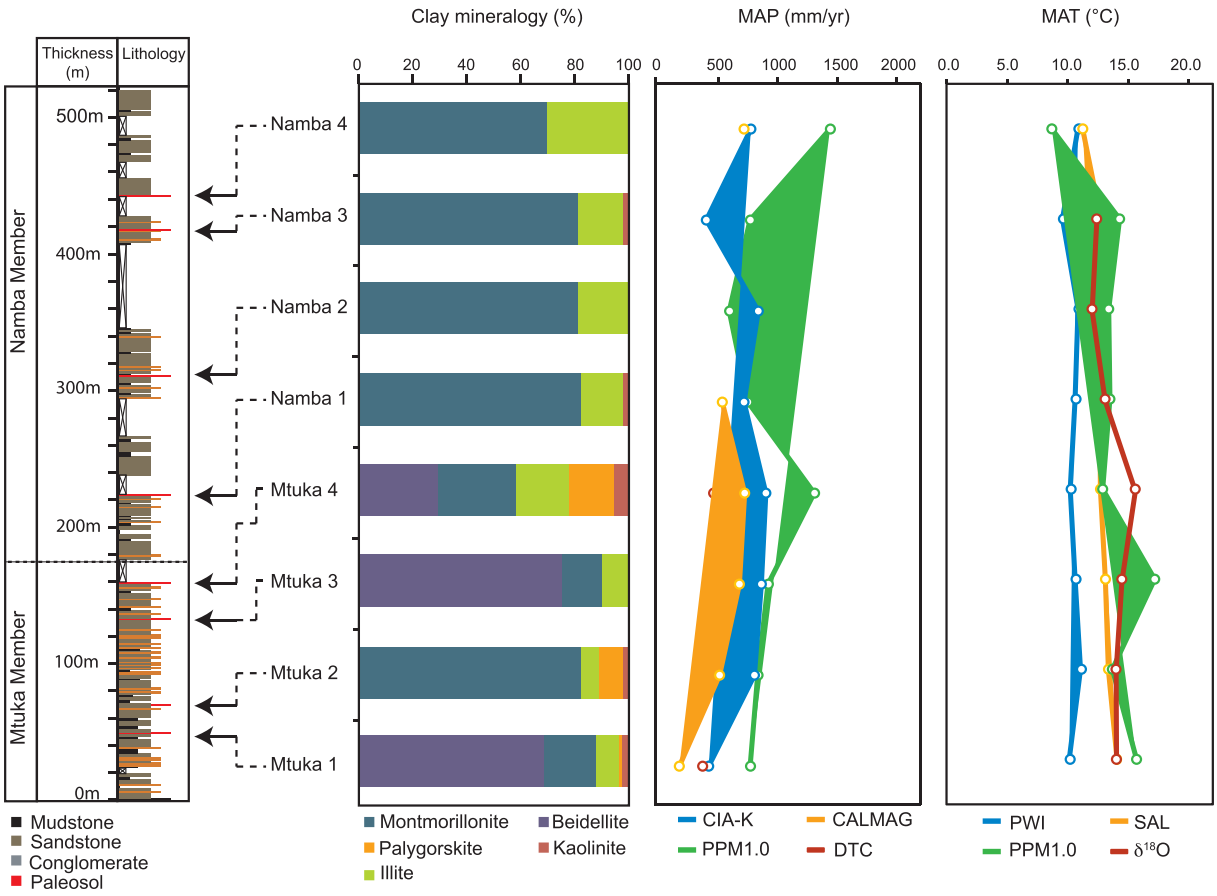

Fig. 8. Clay mineralogy, mean annual precipitation (MAP) and mean annual temperature (MAT) in the Rukwa Rift Basin, estimated from middle and Late Cretaceous paleosols of the Galula Formation. MAP values from chemical index of alteration minus potash (CIA-K) and CALMAG climofunctions, and depth-to carbonate (DTC) and PPM1.0 models. MAT values from paleosol weathering index (PWI) and salinization (SAL) based climofunctions, PPM1.0 spline model and $\delta^{18}O$ of pedogenic carbonates.

rift valley throughout much of the Cretaceous. Subsequent pedogenesis of these fossiliferous successions in the Namba Member also led to the preservation of an important Cretaceous African ichnofauna, which includes evidence of bone-boring insects (Gorscak et al., 2017).

Most of the vertebrate diversity (e.g. the titanosaurian sauropods *Shingopana* and *Rukwatitan* and the crocodyliforms *Pakasuchus* and *Rukwasuchus*) is documented in the Namba Member, with the sauropod dinosaur *Mnyamawamtuka* and the ceratodontid lungfish *Lupaceratodus* representing the two named taxa from the underlying Mtuka Member. Both of the latter taxa are based on only partial specimens, with one (*Lupaceratodus*) based on a single, isolated toothplate. Other terrestrial/freshwater vertebrates have been recovered from the Mtuka Member based on partial, isolated elements (a single, isolated partial crocodyliform femur, isolated sauropod and theropod dinosaur teeth, etc.). Limited invertebrate material has been recovered from the Galula Formation to date, including internal bivalve molds preserving few diagnostic features.

The complex nature of Galula paleosols can be attributed to allogenic factors, such as paleoclimatic shifts, and the natural paleoenvironmental changes in a dynamic fluvial system within a rift setting. During the Cretaceous, global climatic shifts are typically attributed to orbital forcing (e.g. Lehman, 1989; Beckmann et al., 2005; Floegel and Wagner, 2006; Friedrich et al., 2016). In particular, precession and eccentricity are considered controlling factors for intermediate (10^3–10^4 yrs) and longer (10^5 yrs) timescale climate changes (e.g. Lehman, 1989; Salazar-Jaramillo et al., 2019). The 100 kyr and 400 kyr cycles of eccentricity likely influenced the sedimentary cycles of the Galula Formation (Lehman, 1989), and the variations among the Galula paleosols. Eccentricity-driven arid and humid climatic alternations are frequently responsible for sedimentation cycles (Lehman, 1989), with eccentricity maxima associated with enhanced hydrological regimes (Friedrich et al., 2016). Nevertheless, eccentricity is infrequently recorded in fluvial systems, with most changes considered to affect only the lower reaches of a river (Miall, 1991, 2015; Wright and Marriott, 1993). Despite improved age constraints, correlation between eccentricity and the Galula Formation paleosols is not presently feasible.

Evidence of precessional climate forcing, however, may be found in the complexity of the composite and compound paleosols (Aziz et al., 2008). Precessional climate cycles are major drivers of variability in hydrological regimes (Friedrich et al., 2016), capable of causing floods or channel avulsions, and the subsequent rapid and episodic sedimentation observed in the Galula paleosols (Aziz et al., 2008). Intensification of the hydrological cycle, when the northern equinox was coincident with perihelion, is considered responsible for increased fluvial discharges off the coast of Africa during the Late Cretaceous (Beckmann et al., 2005). These precession-driven fluvial discharges led to increased terrigenous input to the oceans, global ocean anoxic events and black shale sedimentation (e.g. Beckmann et al., 2005; Floegel and Wagner, 2006). Episodes of truncation and sedimentation, and development of argillic and carbonate horizons in soils during the Late Cretaceous Namba Member are thought to correspond with these marine sedimentation cycles (e.g. Lehman, 1989).

Although erosion, sedimentation and pedogenesis cycles of the Galula Formation were likely influenced by climatic shifts, deposition of Mtuka and Namba members was primarily initiated by tectonic activity (Roberts et al., 2010). Therefore, truncation and sedimentation episodes

preserved in Galula paleosols may also represent *syn-* and post-rifting sedimentary cycles of the Aptian-Campanian. Roberts et al. (2010) determined that large and variable fluvial discharges leading to the deposition of the Galula Formation were likely linked with periods of climatic shifts, rifting and slow subsidence. Indeed, REE geochemical signatures of each paleosol profile indicate the same provenance throughout the formation, suggesting paleoclimatic variations were the main control on development of paleosol type. Ultimately, the paleosols represent the product of both climate- and tectonic-driven periods of non-deposition interspersed with short-lived episodes of erosion and (re) sedimentation on the large braidplain established across much of the Rukwa Rift.

5.4. Comparison with global studies of Cretaceous climate

Paleosol-derived paleoclimate reconstructions of the middle and Late Cretaceous are sparse in the literature, with the exception of the Maastrichtian. Research has focused on exposed strata in the Bauru (Brazil; e.g. Dal Bo et al., 2009; Delgado et al., 2019), Colville (United States of America (USA); e.g. Flaig et al., 2013; Salazar-Jaramillo et al., 2019), Haţeg (Romania; e.g. Therrien, 2005; Bojar et al., 2009), and Songliao Basins (China; e.g. Huang et al., 2013; Gao et al., 2015), providing valuable paleoclimate inferences for the latest Cretaceous, and the K-T boundary in particular. As a result, comparisons for the paleoclimate data from this study are limited. However, similar cool paleotemperatures (10–15 °C) have been reported during the Early Cretaceous from the Jinlingsi Yangshan (China; Pan and Huang, 2014) and Sichuan Basins (China; Li et al., 2016; Li et al., 2020), from the middle/Late Cretaceous from the Austral/Magallanes (Argentina; Varela et al., 2018) and Western Interior Basins (USA; Retallack and Dilcher, 2012), and the latest Cretaceous from the paleosols of the Haţeg Basin (Romania; Therrien, 2005) and the Deccan Volcanic Province (India; Smith et al., 2015). Each of these paleosol sites was located in the paleo-mid latitudes (~25–50°), similar to that of the Rukwa Rift Basin (~30°S) during the middle/Late Cretaceous (Fig. 9). A study of the Kirkwood Formation paleosols in South Africa estimated a warm to hot climate (25–30 °C) during the Berriasian – Valanginian (Frost, 1996). However quantitative paleosol-derived paleoclimate data from Africa during the middle/Late Cretaceous could not be found in the literature for comparison.

5.5. Comparison with modern climate data

Two possible analogs were identified for comparison of estimated paleoprecipitation and paleotemperature values of the Mtuka (MATμ = 13.3 °C; MAPμ = 710 mm/yr) and Namba (MATμ = 11.9 °C; MAPμ = 767 mm/yr) paleosols with modern climate data from the IAEA global database (Rozanski et al., 1993): Cape Grim (Tanzania) and Zagreb (Croatia). These sites are low-altitude and mid-latitude, and recorded similar values for climate parameters. A third location (Bogota), located at a high-altitude and low-latitude, was discarded as a possible modern analog. The Galula Formation formed at ~30°S, approximately 10° equatorward of present-day Cape Grim (40.7°S) and Zagreb (45.5°N), suggesting the climate during the mid-Cretaceous was similar to but slightly cooler than today. This is consistent with Mtuka paleosols corresponding to the cool greenhouse period that spanned the Aptian-Albian, and Namba paleosols corresponding to Late Cretaceous cooling following the KTM, with no evidence of warmer conditions to indicate that the KTM was preserved in the Galula Formation. It is unsurprising the KTM was not recorded given preservation of fluvial deposits is more likely when there is sufficient accommodation in the system (Wright and Marriott, 1993), with slow generation of accommodation space through much of the depositional history of the Galula Formation (Roberts et al., 2010).

6. Conclusions

Paleosols of the Galula Formation preserve paleoclimatic and paleoenvironmental information about the Early to Late Cretaceous transition (Aptian-Campanian) of Eastern Africa. Mtuka and Namba member soils formed on sub-aerially exposed deposits of a fluvial channel

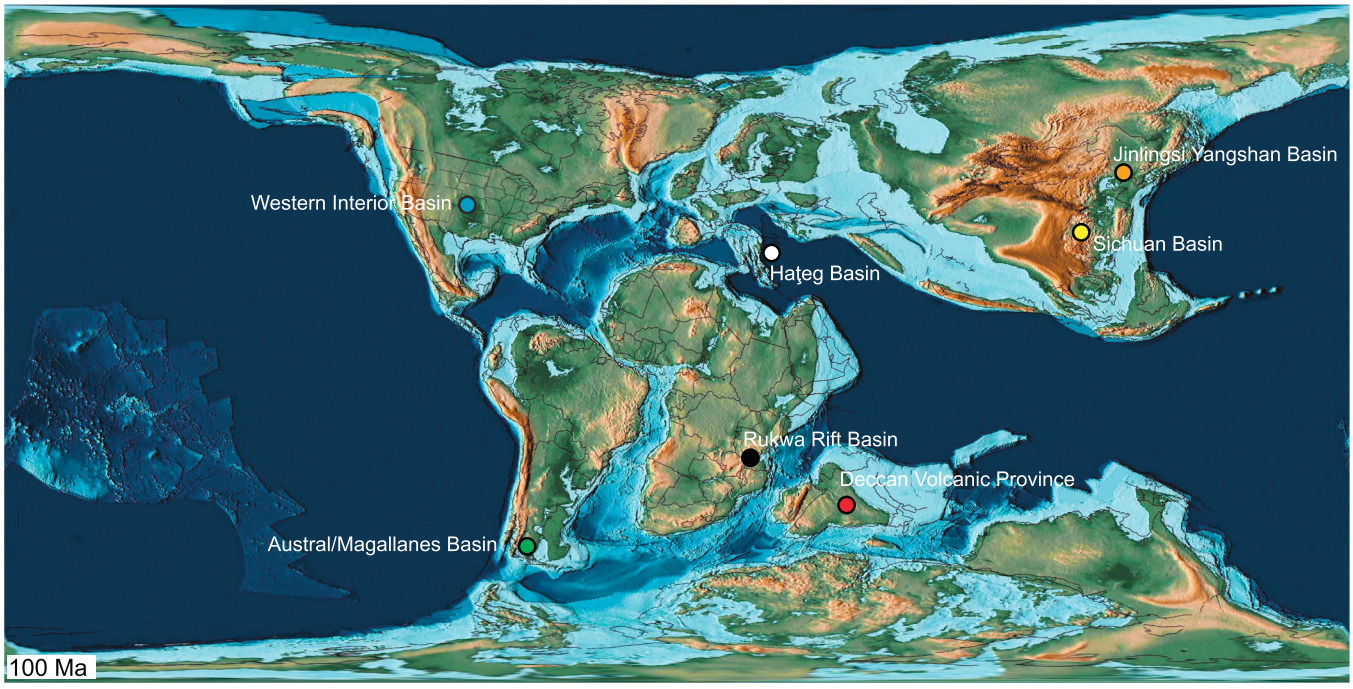

Fig. 9. Location of paleosol sites that recorded cool paleotemperatures (10–15 °C) during the Cretaceous, plotted on an Albian paleogeographic reconstruction (100 Ma), according to Scotese (2016). Black – Rukwa Rift Basin (this study), Blue – Western Interior Basin, Green – Austral/Magallanes Basin, Orange – Jinlingsi Yangshan Basin, Red – Deccan Volcanic Province, White – Haţeg Basin, and Yellow – Sichuan Basin. (For interpretation of the references to colour in this figure legend, the reader is referred to the web version of this article.)

complex, on a dynamic braidplain. Mtuka paleosols developed on channel fill deposits in a semi-arid climate amidst well-defined wet and dry seasons, with the youngest unit (Mtuka 4) forming under the wettest and most seasonal conditions. Paleosols of the overlying Namba Member formed on channel fill and overbank deposits proximal to the main channels, in a semi-arid to sub-humid climate with little seasonality. Taken together, the paleosols of the Galula Formation indicate that the middle/Late Cretaceous was not a continuous greenhouse climate over continental Africa. Rather, temperate conditions prevailed, with evidence of a shift from semi-arid to sub-humid climatic conditions in the region during the Late Cretaceous.

Paleontological, paleomagnetic and sedimentological investigations in the Rukwa Rift Basin have yielded key information on the composition and age of the Galula Formation and its fauna. This study uses paleosols of Rukwa Rift Basin to quantitatively interpret prevailing paleoclimatic and paleoenvironmental conditions during the middle/Late Cretaceous, providing further paleoecological context for the evolution of Cretaceous faunas across continental Africa.

Supplementary data to this article can be found online at https://doi.org/10.1016/j.palaeo.2021.110539.

Declaration of Competing Interest

The authors declare that they have no known competing financial interests or personal relationships that could have appeared to influence the work reported in this paper.

Acknowledgements

We thank E. Maro, A. Tibaijuka, J. Temu, and F. Bassange (Tanzania Antiquties Unit, Dar es Salaam, Tanzania), M. Mashuhuri (Tanzania Commission for Science and Technology), and E. Mshui, N. Boniface, and E. Mbede (University of Dar es Salaam), and L. Kasenagala for assistance with in-country logistics and permits related to field research. We are grateful to the editor and two reviewers for their constructive feedback, which greatly improved the manuscript. This work was supported by the United States National Science Foundation grants [EAR-0617561, BCS-1638796 & EAR-1349825] and the James Cook University W.C. Lacy Scholarship. We would like to thank L. Lawrence for his assistance in the field, as well as the entire paleontological field crews from the Rukwa Rift Basin Project; R. Comley, B. Jones, R.E. Singleton and J. Whan for help in the laboratory.

References

Agyemang, P.C.O., Roberts, E.M., Downie, B., Sertich, J.J., 2019. Sedimentary provenance and maximum depositional age analysis of the Cretaceous? Lapur and Muruanachok sandstones (Turkana Grits), Turkana Basin, Kenya. Geol. Mag. 156, 1334–1356.

Alekseeva, T., Alekseev, A., Kalinin, P., 2018. The Mississippian Paleosols in the Brontsy Quarry, Kaluga region. Eur. Soil Sci. 51, 744–757.

Ashley, G.M., Driese, S.G., 2000. Paleopedology and paleohydrology of a volcaniclastic paleosol interval: implications for early Pleistocene stratigraphy and paleoclimate record, Olduvai Gorge, Tanzania. J. Sediment. Res. 70, 1065–1080.

Aslan, A., Autin, W.J., 1998. Holocene flood-plain soil formation in the southern lower Mississippi Valley: implications for interpreting alluvial paleosols. Geol. Soc. Am. Bull. 110, 433–449.

Aziz, H.A., Hilgen, F.J., Van Luijk, G.M., Sluijs, A., Kraus, M.J., Pares, J.M., Gingerich, P. D., 2008. Astronomical climate control on paleosol stacking patterns in the upper Paleocene–lower Eocene Willwood Formation, Bighorn Basin, Wyoming. Geology 36, 531–534.

Bau, M., 1991. Rare-earth element mobility during hydrothermal and metamorphic fluid-rock interaction and the significance of the oxidation state of europium. Chem. Geol. 93, 219–230.

Beckmann, B., Flögel, S., Hofmann, P., Schulz, M., Wagner, T., 2005. Orbital forcing of Cretaceous river discharge in tropical Africa and ocean response. Nature 437, 8.

Birkeland, P.W., 1999. Soils and Geomorphology. Oxford University Press, New York.

Bojar, A.V., Ottner, F., Bojar, H.P., Grigorescu, D., Persoiu, A., 2009. Stable isotope and mineralogical investigations on clays from the Late Cretaceous sequences, Haţeg Basin, Romania. Appl. Clay Sci. 45, 155–163.

Borchardt, G., 1989. Smectites. Miner. Soil Environ. 1, 675–727.

Bowman, V.C., Francis, J.E., Riding, J.B., 2013. Late Cretaceous winter sea ice in Antarctica? Geology 41, 1227–1230.

Bown, T.M., Kraus, M.J., 1987. Integration of channel and floodplain suites, I. Developmental sequence and lateral relations of alluvial paleosols. J. Sediment. Res. 57.

Breecker, D., Sharp, Z., Mcfadden, L.D., 2009. Seasonal bias in the formation and stable isotopic composition of pedogenic carbonate in modern soils from Central New Mexico, USA. GSA Bull. 121, 630–640.

Bull, W.B., 1991. Geomorphic Responses to Climatic Change. Oxford University Press, New York.

Burgener, L., Hyland, E., Huntington, K.W., Kelson, J.R., Sewall, J.O., 2019. Revisiting the equable climate problem during the Late Cretaceous greenhouse using paleosol carbonate clumped isotope temperatures from the Campanian of the Western Interior Basin, USA. Palaeogeogr. Palaeoclimatol. Palaeoecol. 516, 244–267.

Chorowicz, J., 2005. The east African rift system. J. Afr. Earth Sci. 43, 379–410.

Da Silva, M.L., Batezelli, A., Ladeira, F.S.B., 2017. The mineralogy of paleosols in the Marilia Formation and their importance in the environmental evolution of the Maastrichtian of the Bauru Basin in southeastern Brazil. Br. J. Geol. 47, 403–426.

Da Silva, M.L., Batezelli, A., Ladeira, F.S.B., 2018. Genesis and paleoclimatic significance of palygorskite in the cretaceous paleosols of the Bauru Basin, Brazil. Catena 168, 110–128.

Dal Bo, P.F.F., Basilici, G., Angelica, R.S., Ladeira, F.S.B., 2009. Paleoclimatic interpretations from pedogenic calcretes in a Maastrichtian semi-arid eolian sand-sheet palaeoenvironment: Marilia Formation (Bauru Basin, southeastern Brazil). Cretac. Res. 30, 659–675.

Delgado, L., Batezelli, A., Ladeira, F.S.B., Luna, J., 2019. Paleoenvironmental and paleoclimatic interpretation of the Late Cretaceous Marllia Formation (Brazil) based on paleosol geochemistry. Catena 180, 365–382.

Delvaux, D., Kervyn, F., Vittori, E., Kajara, R., Kilembe, E., 1998. Late Quaternary tectonic activity and lake level change in the Rukwa Rift Basin. J. Afr. Earth Sci. 26, 397–421.

Driese, S.G., Ashley, G.M., 2016. Paleoenvironmental reconstruction of a paleosol catena, the Zinj archeological level, Olduvai Gorge, Tanzania. Quat. Res. 85, 133–146.

Driese, S.G., Peppe, D.J., Beverly, E.J., Dipietro, L.M., Arellano, L.N., Lehmann, T., 2016. Paleosols and paleoenvironments of the early Miocene deposits near Karungu, Lake Victoria, Kenya. Palaeogeogr. Palaeoclimatol. Palaeoecol. 443, 167–182.

Dworkin, S., Nordt, L., Atchley, S., 2005. Determining terrestrial paleotemperatures using the oxygen isotopic composition of pedogenic carbonate. Earth Planet. Sci. Lett. 237, 56–68.

Ebinger, C., 1989. Tectonic development of the western branch of the East African rift system. Geol. Soc. Am. Bull. 101, 885–903.

Ebinger, C., Deino, A., Drake, R., Tesha, A., 1989. Chronology of volcanism and rift basin propagation: Rungwe volcanic province, East Africa. J. Geophys. Res. Solid Earth 94, 15785–15803.

Fawley, A., James, T., 1955. A pyrochlore (columbium) carbonatite, southern Tanganyika. Econ. Geol. 50, 571–585.

Flaig, P.P., Mccarthy, P.J., Fiorillo, A.R., 2013. Anatomy, evolution, and paleoenvironmental interpretation of an ancient Arctic coastal plain: Integrated paleopoedology and palynology from the Upper Cretaceous (Maastrichtian) Prince Creek Formation, North Slope, Alaska, USA. In: Driese, S.G., Nordt, L.C. (Eds.), New Frontiers in Paleopedology and Terrestrial Paleoclimatology: Paleosols and Soil Surface Analog Systems.

Floegel, S., Wagner, T., 2006. Insolation-control on the Late Cretaceous hydrological cycle and tropical African climate—global climate modelling linked to marine climate records. Palaeogeogr. Palaeoclimatol. Palaeoecol. 235, 288–304.

Friedrich, O., Batenburg, S. J., Moriya, K., Voigt, S., Cournède, C., Möbius, I., Blum, P., Bornemann, A., Fiebig, J., Hasegawa, T., Hull, P. M., Norris, R. D., Röhl, U., Westerhold, T., Wilson, P. A., and IODP Expedition: Maastrichtian carbon isotope stratigraphy and cyclostratigraphy of the Newfoundland Margin (Site U1403, IODP Leg 342), Clim. Past Discuss. [preprint], https://doi.org/10.5194/cp-2016-51, 2016.

Frost, S., 1996. Early Cretaceous Alluvial Palaeosols (Kirkwood Formation, Algoa Basin, South Africa) and their Palaeoenvironmental and Palaeoclimatological Significance. Unpublished M.Sc. thesis. Rhodes University.

Gallagher, T.M., Sheldon, N.D., 2013. A new paleothermometer for forest paleosols and its implications for Cenozoic climate. Geology 41, 647–650.

Gao, Y., Ibarra, D.E., Wang, C., Caves, J.K., Chamberlain, C.P., Graham, S.A., Wu, H., 2015. Mid-latitude terrestrial climate of East Asia linked to global climate in the Late Cretaceous. Geology 43, 287–290.

Gile, L.H., Peterson, F.F., Grossman, R.B., 1966. Morphological and genetic sequences of carbonate accumulation in desert soils. Soil Sci. 101, 347–360.

Gorscak, E., O'Connor, P.M., 2019. A new African Titanosaurian Sauropod Dinosaur from the middle Cretaceous Galula Formation (Mtuka Member), Rukwa Rift Basin, Southwestern Tanzania. PLoS One 14, e0211412.

Gorscak, E., O'Connor, P.M., Stevens, N.J., Roberts, E.M., 2014. The basal titanosaurian Rukwatitan bisepultus (Dinosauria, Sauropoda) from the middle Cretaceous Galula Formation, Rukwa Rift Basin, southwestern Tanzania. J. Vertebr. Paleontol. 34, 1133–1154.

Gorscak, E., O'Connor, P.M., Roberts, E.M., Stevens, N.J., 2017. The second titanosaurian (Dinosauria: Sauropoda) from the middle Cretaceous Galula Formation, southwestern Tanzania, with remarks on African titanosaurian diversity. J. Vertebr. Paleontol. 37, e1343250.

Gottfried, M.D., O'Connor, P.M., Jackson, F.D., Roberts, E.M., Chami, R., 2004. Dinosaur eggshell from the Red Sandstone group of Tanzania. J. Vertebr. Paleontol. 24, 494–497.

Gottfried, M.D., Stevens, N.J., Roberts, E.M., O'Connor, P.M., Chami, R., 2009. A new Cretaceous lungfish (Dipnoi: Ceratodontidae) from the Rukwa Rift Basin, Tanzania. Afr. Nat. Hist. 5, 31–36.
Guiraud, R., Binks, R.M., Fairhead, J.D., Wilson, M., 1992. Chronology and geodynamic setting of Cretaceous-Cenozoic rifting in West and Central Africa. Tectonophysics 213, 227–234.
Hamer, J., Sheldon, N., Nichols, G., Collinson, M., 2007. Late Oligocene–early Miocene paleosols of distal fluvial systems, Ebro Basin, Spain. Palaeogeogr. Palaeoclimatol. Palaeoecol. 247, 220–235.
Hembree, D.I., Bowen, J.J., 2017. Paleosols and ichnofossil of the Upper Pennsylvanian-Lowe Monongahela and Dunkard Groups (OHIO, USA): a multi-proxy approach to unravelling complex variability in ancient terrestrial landscapes. Palaios 32, 295–320.
Hembree, D.I., Hasiotis, S.T., 2007. Paleosols and ichnofossils of the White River Formation of Colorado: Insight into soil ecosystems of the North American Midcontinent during the Eocene-Oligocene transition. Palaios 22, 123–142.
Hilbert-Wolf, H.L., Roberts, E.M., 2015. Giant seismites and megablock uplift in the East African Rift: evidence for late Pleistocene large magnitude earthquakes. PLoS One 10, e0129051.
Hilbert-Wolf, H.L., Roberts, E.M., Simpson, E.L., 2016. New sedimentary structures in seismites from SW Tanzania: evaluating gas-vs. water-escape mechanisms of soft-sediment deformation. Sediment. Geol. 344, 253–262.
Hilbert-Wolf, H., Roberts, E., Downie, B., Mtelela, C., Stevens, N.J., O'Connor, P., 2017. Application of U–Pb detrital zircon geochronology to drill cuttings for age control in hydrocarbon exploration wells: a case study from the Rukwa Rift Basin, Tanzania. AAPG Bull. 101, 143–159.
Huang, C., Retallack, G.J., Wang, C., 2012. Early Cretaceous atmospheric pCO 2 levels recorded from pedogenic carbonates in China. Cretac. Res. 33, 42–49.
Huang, C., Retallack, G.J., Wang, C., Huang, Q., 2013. Paleoatmospheric pCO 2 fluctuations across the Cretaceous–Tertiary boundary recorded from paleosol carbonates in NE China. Palaeogeogr. Palaeoclimatol. Palaeoecol. 385, 95–105.
Huber, B.T., Macleod, K.G., Watkins, D.K., Coffin, M.F., 2018. The rise and fall of the Cretaceous Hot Greenhouse climate. Glob. Planet. Chang. 167, 1–23.
Hyland, E.G., Sheldon, N.D., 2013. Coupled CO_2-climate response during the early Eocene climatic optimum. Palaeogeogr. Palaeoclimatol. Palaeoecol. 369, 125–135.
Jacobs, L., 1990. The dinosaur beds of northern Malawi, Africa. Natl. Geogr. Res. 6, 196–203.
Johnson, T.A., 2004. Stratigraphy, Depositional Environments, and Coalbed Gas Potential of Middle Pennsylvanian (Desmoinesian Stage) Coals-Bourbon Arch Region, Eastern Kansas. University of Kansas, Geology.
Khademi, H., Mermut, A., 1999. Submicroscopy and stable isotope geochemistry of carbonates and associated palygorskite in Iranian Aridisols. Eur. J. Soil Sci. 50, 207–216.
Khormali, F., Abtahi, A., 2003. Origin and distribution of clay minerals in calcareous arid and semi-arid soils of Fars Province, southern Iran. Clay Miner. 38, 511–527.
Kilembe, E.A., Rosendahl, B., 1992. Structure and stratigraphy of the Rukwa rift. Tectonophysics 209, 143–158.
Kjennerud, T., Lippard, S., Vanhauwaert, P., 2001. Short term development of intracontinental rifts, with reference to the late Quaternary of the Rukwa Rift (East African Rift System). Mar. Pet. Geol. 18, 307–317.
Klappa, C.F., 1980a. Brecciation textures and tepee structures in Quaternary calcrete (caliche) profiles from eastern Spain: the plant factor in their formation. Geol. J. 15, 81–89.
Klappa, C.F., 1980b. Rhizoliths in terrestrial carbonates: classification, recognition, genesis and significance. Sedimentology 27, 613–629.
Köppen, W.P., 1923. Die Klimate der Erde: Grundriss der Klimakunde. Walter de Gruyter.
Kraus, M.J., 1999. Paleosols in clastic sedimentary rocks: their geologic applications. Earth Sci. Rev. 47, 41–70.
Kraus, M.J., Hasiotis, S.T., 2006. Significance of different modes of rhizolith preservation to interpreting paleoenvironmental and paleohydrologic settings: examples from Paleogene paleosols, Bighorn Basin, Wyoming, USA. J. Sediment. Res. 76, 633–646.
Kraus, M.J., Riggins, S., 2007. Transient drying during the Paleocene–Eocene Thermal Maximum (PETM): analysis of paleosols in the Bighorn Basin, Wyoming. Palaeogeogr. Palaeoclimatol. Palaeoecol. 245, 444–461.
Lawrence, L., Spandler, C., Roberts, E., Hilbert-Wolf, H., 2020. Mineralogy and origin of the alkaline Nsungwe Formation tuffs of the Rukwa Rift Basin, southwestern Tanzania. Lithos 105885.
Lehman, T.M., 1989. Upper cretaceous (Maastrichtian) paleosols in Trans-Pecos Texas. Geol. Soc. Am. Bull. 101, 188–203.
Li, J., Wen, X., Huang, C., 2016. Lower Cretaceous paleosols and paleoclimate in Sichuan Basin, China. Cretac. Res. 62, 154–171.
Li, J., Wen, X., Huang, C., 2020. Lower and upper Cretaceous paleosols in the western Sichuan Basin, China: Implications for regional paleoclimate. Geol. J. 55, 390–408.
Mack, G.H., James, W.C., 1992. Calcic paleosols of the Plio-Pleistocene Camp Rice and Palomas Formations, southern Rio Grande rift, USA. Sediment. Geol. 77, 89–109.
Mack, G.H., James, W., 1994. Paleoclimate and the global distribution of paleosols. J. Geol. 102, 360–366.
Mack, G.H., James, W.C., Monger, H.C., 1993. Classification of paleosols. Geol. Soc. Am. Bull. 105, 129–136.
Marriott, S., Wright, V., 1993. Palaeosols as indicators of geomorphic stability in two Old Red Sandstone alluvial suites, South Wales. J. Geol. Soc. 150, 1109–1120.
Maynard, J., 1992. Chemistry of modern soils as a guide to interpreting Precambrian paleosols. J. Geol. 100, 279–289.
Mccarthy, P.J., Plint, A.G., 1998. Recognition of interfluve sequence boundaries: integrating paleopedology and sequence stratigraphy. Geology 26, 387–390.
Mclennan, S.M., 2001. Relationships between the trace element composition of sedimentary rocks and upper continental crust. Geochem. Geophys. Geosyst. 2.
Miall, A.D., 1991. Stratigraphic sequences and their chronostratigraphic correlation. J. Sediment. Res. 61 (4), 497–505.
Miall, A.D., 2015. Updating Uniformitarianism: stratigraphy as just a set of 'frozen accidents'. Geol. Soc. Lond., Spec. Publ. 404, 11–36.
Mohanty, S.P., Nanda, S., 2016. Geochemistry of a paleosol horizon at the base of the Sausar Group, Central India: implications on atmospheric conditions at the Archean–Paleoproterozoic boundary. Geosci. Front. 7, 759–773.
Morley, C., Cunningham, S., Harper, R., Wescott, W.A., 1992. Geology and geophysics of the Rukwa rift, East Africa. Tectonics 11, 69–81.
Mtelela, C., Roberts, E.M., Downie, R., Hendrix, M.S., 2016. Interplay of structural, climatic, and volcanic controls on Late Quaternary Lacustrine–Deltaic sedimentation patterns in the Western Branch of the East African Rift System, Rukwa Rift Basin, Tanzania. J. Sediment. Res. 86, 1179–1207.
Mtelela, C., Roberts, E.M., Hilbert-Wolf, H.L., Downie, R., Hendrix, M.S., O'Connor, P.M., Stevens, N.J., 2017. Sedimentology and paleoenvironments of a new fossiliferous late Miocene-Pliocene sedimentary succession in the Rukwa Rift Basin, Tanzania. J. Afr. Earth Sci. 129, 260–281.
Munsell Color, 2009. Munsell Soil Color Charts, Revised ed. Macbeth, Division of Kollmorgen Instruments Corp, Newburgh, New York.
Nesbitt, H., Young, G., 1982. Early Proterozoic climates and plate motions inferred from major element chemistry of lutites. Nature 299, 715–717.
Nettleton, W., Peterson, F., 1983. Aridisols. In: Devezlopments in Soil Science. Elsevier.
Nordt, L., Driese, S., 2010. New weathering index improves paleorainfall estimates from Vertisols. Geology 38, 407–410.
Nordt, L., Atchley, S., Dworkin, S., 2003. Terrestrial evidence for two greenhouse events in the latest Cretaceous. GSA Today 13, 4–9.
Nordt, L., Orosz, M., Driese, S., Tubbs, J., 2006. Vertisol carbonate properties in relation to mean annual precipitation: implications for paleoprecipitation estimates. J. Geol. 114, 501–510.
O'Connor, P.M., Gottfried, M.D., Stevens, N.J., Roberts, E.M., Ngasala, S., Kapilima, S., Chami, R., 2006. A new vertebrate fauna from the Cretaceous Red Sandstone Group, Rukwa Rift Basin, southwestern Tanzania. J. Afr. Earth Sci. 44, 277–288.
O'Connor, P.M., Sertich, J.J., Stevens, N.J., Roberts, E.M., Gottfried, M.D., Hieronymus, T.L., Jinnah, Z.A., Ridgely, R., Ngasala, S.E., Temba, J., 2010. The evolution of mammal-like crocodyliforms in the Cretaceous Period of Gondwana. Nature 466, 748–751.
O'Connor, P.M., Krause, D.W., Stevens, N.J., Groenke, J.R., Macphee, R.D., Kalthoff, D. C., Roberts, E.M., 2019. A new mammal from the Turonian–Campanian (Upper Cretaceous) Galula Formation, southwestern Tanzania. Acta Palaeontol. Pol. 64.
Pan, Y.Y., Huang, C.M., 2014. Quantitative reconstruction of early cretaceous paleoclimate using paleosol carbonates in China. Carbonates Evaporites 29, 327–335.
Paquet, H., Millot, G., 1972. Geochemical evolution of clay minerals in the weathered products in soils of Mediterranean climate. In: Proceedings of the International Clay Conference, pp. 199–202. Madrid.
Pearson, P.N., Nicholas, C.J., Singano, J.M., Bown, P.R., Coxall, H.K., Van Dongen, B.E., Huber, B.T., Karega, A., Lees, J.A., Msaky, E., 2004. Paleogene and cretaceous sediment cores from the Kilwa and Lindi areas of coastal Tanzania: Tanzania Drilling Project Sites 1–5. J. Afr. Earth Sci. 39, 25–62.
PiPujol, M.D., Buurman, P., 1997. Dynamics of iron and calcium carbonate redistribution and palaeohydrology in middle Eocene alluvial paleosols of the Southeast Ebro Basin margin (Catalonia, Northeast Spain). Palaeogeogr. Palaeoclimatol. Palaeoecol. 134, 87–107.
Retallack, G.J., 1997. Colour Guide to Paleosols. John Wiley & Sons Ltd.
Retallack, G.J., 2001. Soils of the Past: An Introduction to Paleopedology. Blackwell Science, Oxford.
Retallack, G.J., 2003. Soils and global change in the carbon cycle over geological time. Treat. Geochem. 5, 605.
Retallack, G.J., 2005. Pedogenic carbonate proxies for amount and seasonality of precipitation in paleosols. Geology 33, 333–336.
Retallack, G.J., Dilcher, D.L., 2012. Outcrop versus core and geophysical log interpretation of mid-Cretaceous paleosols from the Dakota Formation of Kansas. Palaeogeogr. Palaeoclimatol. Palaeoecol. 329-330, 47–63.
Roberts, E.M., O'connor, P.M., Gottfried, M.D., Stevens, N., Kapalima, S., Ngasala, S., 2004. Revised stratigraphy and age of the Red Sandstone Group in the Rukwa Rift Basin, Tanzania. Cretac. Res. 25, 749–759.
Roberts, E.M., O'connor, P.M., Stevens, N.J., Gottfried, M.D., Jinnah, Z.A., Ngasala, S., Choh, A.M., Armstrong, R.A., 2010. Sedimentology and depositional environments of the Red Sandstone Group, Rukwa Rift Basin, southwestern Tanzania: new insight into Cretaceous and Paleogene terrestrial ecosystems and tectonics in sub-equatorial Africa. J. Afr. Earth Sci. 57, 179–212.
Roberts, E.M., Stevens, N., O'Connor, P., Dirks, P., Gottfried, M.D., Clyde, W., Armstrong, R., Kemp, A., Hemming, S., 2012. Initiation of the western branch of the East African Rift coeval with the eastern branch. Nat. Geosci. 5, 289.
Roberts, E.M., Todd, C.N., Aanen, D.K., Nobre, T., Hilbert-Wolf, H.L., O'Connor, P.M., Tapanila, L., Mtelela, C., Stevens, N.J., 2016. Oligocene termite nests with in situ fungus gardens from the Rukwa Rift Basin, Tanzania, support a Paleogene African origin for insect agriculture. PLoS One 11, e0156847.
Rosendahl, B., Kilembe, E., Kaczmarick, K., 1992. Comparison of the Tanganyika, Malawi, Rukwa and Turkana Rift zones from analyses of seismic reflection data. Tectonophysics 213, 235–256.
Rozanski, K., Araguás-Araguás, L., Gonfiantini, R., 1993. Isotopic patterns in modern global precipitation. GMS 78, 1–36.

Salazar-Jaramillo, S., Mccarthy, P.J., Ochoa, A., Fowell, S.J., Longstaffe, F.J., 2019. Paleoclimate reconstruction of the Prince Creek Formation, Arctic Alaska, during Maastrichtian global warming. Palaeogeogr. Palaeoclimatol. Palaeoecol. 532.
Scotese, C.R., 2016. PALEOMAP PaleoAtlas for GPlates and the PaleoData Plotter Program, PALEOMAP Project, https://www.earthbyte.org/paleomap-paleoatlas-for-gplates/ DOI: 10.13140/RG2.2.34367.00166 accessed on 01.09.2020.
Sertich, J.J., O'Connor, P.M., 2014. A new crocodyliform from the middle Cretaceous Galula Formation, southwestern Tanzania. J. Vertebr. Paleontol. 34, 576–596.
Sheldon, N.D., 2006a. Quaternary glacial-interglacial climate cycles in Hawaii. J. Geol. 114, 367–376.
Sheldon, N.D., 2006b. Abrupt chemical weathering increase across the Permian–Triassic boundary. Palaeogeogr. Palaeoclimatol. Palaeoecol. 231, 315–321.
Sheldon, N.D., Retallack, G.J., 2001. Equation for compaction of paleosols due to burial. Geology 29, 247–250.
Sheldon, N.D., Tabor, N.J., 2009. Quantitative paleoenvironmental and paleoclimatic reconstruction using paleosols. Earth Sci. Rev. 95, 1–52.
Sheldon, N.D., Retallack, G.J., Tanaka, S., 2002. Geochemical climofunctions from North American soils and application to paleosols across the Eocene-Oligocene boundary in Oregon. J. Geol. 110, 687–696.
Smith, J.J., Hasiotis, S.T., Woody, D.T., Kraus, M.J., 2008. Paleoclimatic implications of crayfish-mediated prismatic structures in paleosols of the Paleogene Willwood Formation, Bighorn Basin, Wyoming, USA. J. Sediment. Res. 78, 323–334.
Smith, S.Y., Manchester, S.R., Samant, B., Mohabey, D.M., Wheeler, E., Baas, P., Kapgate, D., Srivastava, R., Sheldon, N.D., 2015. Integrating paleobotanical, paleosol, and stratigraphic data to study critical transitions: a case study from the Late Cretaceous–Paleocene of India. Paleontol. Soc. Paper 21, 137–166.
Stevens, N.J., O'Connor, P.M., Gottfried, M.D., Roberts, E.M., Ngasala, S., 2005. An anthropoid primate humerus from the Rukwa Rift Basin, Paleogene of southwestern Tanzania. J. Vertebr. Paleontol. 25, 986–989.
Stevens, N.J., O'Connor, P.M., Gottfried, M.D., Roberts, E.M., Ngasala, S., Dawson, M.R., 2006. Metaphiomys (Rodentia: Phiomyidae) from the Paleogene of southwestern Tanzania. J. Paleontol. 80, 407–410.
Stevens, N.J., Gottfried, M.D., Roberts, E.M., Kapilima, S., Ngasala, S., O'Connor, P.M., 2008. Paleontological exploration in Africa. In: Elwyn Simons: A Search for Origins. Springer.
Stevens, N.J., Holroyd, P.A., Roberts, E.M., O'Connor, P.M., Gottfried, M.D., 2009. Kahawamys mbeyaensis (n. gen., n. sp.)(Rodentia: Thryonomyoidea) from the late Oligocene Rukwa Rift Basin, Tanzania. J. Vertebr. Paleontol. 29, 631–634.
Stevens, N.J., Seiffert, E.R., O'Connor, P.M., Roberts, E.M., Schmitz, M.D., Krause, C., Gorscak, E., Ngasala, S., Hieronymus, T.L., Temu, J., 2013. Palaeontological evidence for an Oligocene divergence between Old World monkeys and apes. Nature 497, 611–614.
Stinchcomb, G.E., Nordt, L.C., Driese, S.G., Lukens, W.E., Williamson, F.C., Tubbs, J.D., 2016. A data-driven spline model designed to predict paleoclimate using paleosol geochemistry. Am. J. Sci. 316, 746–777.
Tabor, N.J., Myers, T.S., 2015. Paleosols as indicators of paleoenvironment and paleoclimate. Annu. Rev. Earth Planet. Sci. 43, 333–361.
Tabor, N.J., Montañez, I.P., Zierenberg, R., Currie, B.S., 2004. Mineralogical and geochemical evolution of a basalt-hosted fossil soil (Late Triassic, Ischigualasto Formation, Northwest Argentina): potential for paleoenvironmental reconstruction. Geol. Soc. Am. Bull. 116, 1280–1293.
Taylor, S.R., Mclennan, S.M., 1985. The Continental Crust: Its Composition and Evolution.
Therrien, F., 2005. Palaeoenvironments of the latest cretaceous (Maastrichtian) dinosaurs of Romania: insights from fluvial deposits and paleosols of the Transylvanian and Haţeg basins. Palaeogeogr. Palaeoclimatol. Palaeoecol. 218, 15–56.
Therrien, F., Zelenitsky, D.K., Weishampel, D.B., 2009. Palaeoenvironmental reconstruction of the Late Cretaceous Sanpetru Formation (Haţeg Basin, Romania) using paleosols and implications for the "disappearance" of dinosaurs. Palaeogeogr. Palaeoclimatol. Palaeoecol. 272, 37–52.
Thornburg, J.D., Miller, K.G., Browning, J.V., Wright, J.D., 2019. Mid-Cretaceous paleopedology and landscape reconstruction of the Mid-Atlantic U.S. Coastal Plain. J. Sediment. Res. 89, 253–272.
United States Natural Resources Conservation, S, 1999. Soil Taxonomy: A Basic System of Soil Classification for Making and Interpreting Soil Surveys. U.S. Dept. of Agriculture, Natural Resources Conservation Service, Washington, DC.
Van Breemen, N., 1975. Acidification and deacidification of coastal plain soils as a result of periodic flooding. Soil Sci. Soc. Am. J. 39, 1153–1157.
Varela, A.N., Raigemborn, M.S., Richiano, S., White, T., Poiré, D.G., Lizzoli, S., 2018. Late Cretaceous paleosols as paleoclimate proxies of high-latitude Southern Hemisphere: Mata Amarilla Formation, Patagonia, Argentina. Sediment. Geol. 363, 83–95.
Widlansky, S.J., Clyde, W.C., O'Connor, P.M., Roberts, E.M., Stevens, N.J., 2018. Paleomagnetism of the Cretaceous Galula Formation and implications for vertebrate evolution. J. Afr. Earth Sci. 139, 403–420.
Wright, V.P., Marriott, S.B., 1993. The sequence stratigraphy of fluvial depositional systems: the role of floodplain sediment storage. Sediment. Geol. 86, 203–210.